UNIVERSITÀ DI SIENA 1240

University of Siena
Department of Medical Biotechnologies

Doctorate in Genetics, Oncology and Clinical Medicine (GenOMeC)
XXXV Cycle (2019-2022)
Coordinator: Prof. Francesca Ariani

Approaching PCDH19 clustering epilepsy *in vitro*: CRISPR/Cas9-mediated gene editing and characterization of patient-derived hiPSC-neurons

Scientific disciplinary sector: BIO/11 – Molecular Biology

PhD candidate:

Diana Alaverdian

Tutor:
Prof. Elisa Frullanti, Prof. Ilaria Meloni
University of Siena

Supervisor:
Dr. Silvestro Conticello
University of Florence

Academic year
2022/23

Summary

List of Figures

List of Tables

Abstract

Loss of function mutations in *PCDH19* gene cause an X-linked, infant-onset clustering epilepsy, associated with intellectual disability and autistic features. The unique pattern of inheritance includes random X-chromosome inactivation, which leads to pathological tissue mosaicism. Females carrying *PCDH19* mutations are affected, while males have normal phenotype. No cure is presently available for this disease.

We obtained heterozygous cells from the affected patient and performed transfection experiments creating two double-strand breaks and deleting the intervening DNA segment of *PCDH19* gene. We generated a CRISPR/Cas9 mediated knockout of the *PCDH19* gene in patient-derived cells. Targeting different parts of the *PCDH19* gene, we obtained 72,9% of editing efficiency using the AAV-based vector with sgRNAs flanking the ends of the first exon, and with sgRNAs flanking the ends of the gene – 48,5%, employing a lentivirus-based vector.

Fibroblasts from a female patient carrying frameshift mutation c.2133delG were reprogrammed into human induced pluripotent stem cells (hiPSC). We created a cell model of PCDH19-clustering epilepsy (PCDH19-CE) where both cell populations co-exist, by mixing wild-type and mutated human iPSC clones, and differentiated them into mature neurons with overexpression of the transcriptional factor Neurogenin 2. We set up the conditions for neuronal differentiation of hiPSC using an overexpression with transcriptional factor Neurogenin 2. With a preliminary electrophysiological experiment we observed that *PCDH19* mosaic neurons tend to have an elevated excitability, representing the situation in PCDH19-CE brain. We confirmed and completed existing data showing that *PCDH19* mutation c.2133delG affects proper metaphases and leads to an increased number of centrosomes in stem cells.

In conclusion, we provide an efficient and reproducible strategy of CRISPR/Cas9 targeted *PCDH19* knockout and demonstrate that this is a promising therapeutic tool for the treatment of PCDH19-CE. We

suggest Ngn-2 hiPSC-derived PCDH19 neurons as an informative, efficient, and reproducible experimental tool for understanding the pathogenesis of PCDH19-CE and a suitable approach for use in targeted drug screening strategies.

Introduction

PCDH19-CE genetics, clinics, and mechanism

Protocadherin 19 *(PCDH19)* is one of the genes which pathogenic variant mosaicism causes epilepsy-related neurodevelopmental disorder [1] and is the second most relevant gene in epilepsy after *SCN1A* [2]. Heterozygous loss-of-function (LOF) mutations in *PCDH19* located on the X-chromosome cause an epileptic encephalopathy characterized by seizure onset in infancy, mild to severe intellectual disability (ID),often accompanied by Autistic Spectrum Disorders (ASD), and psychosis [3].

PCDH19 gene is located on the short arm of the X-chromosome (Xq22.1). Different from the most X-linked diseases, the PCDH19 epilepsy demonstrates a unique pattern of inheritance. The disease is caused by a random X-chromosome inactivation, which leads to tissue mosaicism where the part of the cells expresses wild-type *PCDH19* and part – mutant *PCDH19*. Males carrying *PCDH19* mutations have normal phenotype without seizures and ID while females are affected. This mechanism is so-called "cellular interference" implying that the disease mechanism is based on co-existence of two populations of cells, one expressing the wild-type and the other the mutant allele (**Figure 1A**) [4].

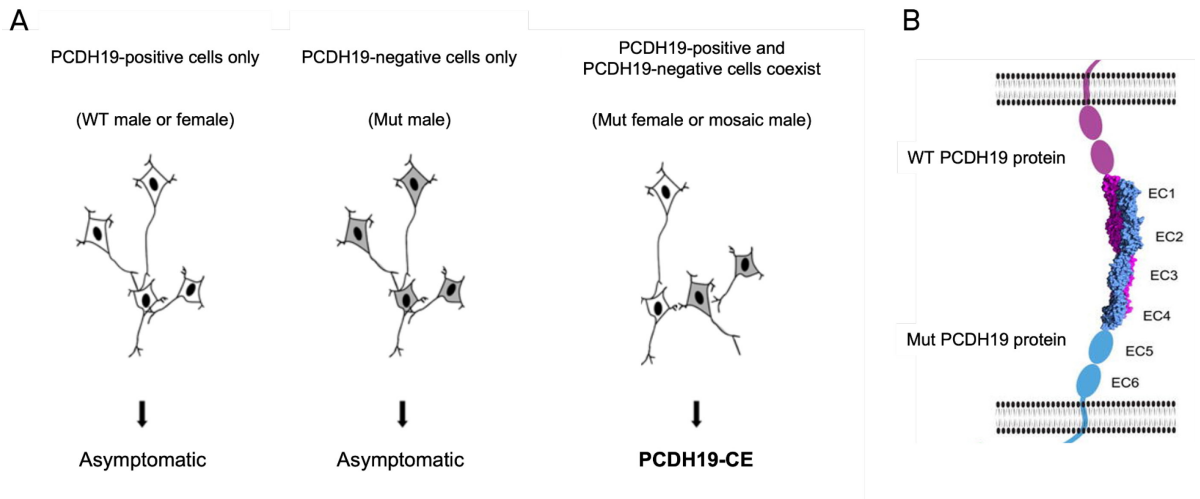

Figure 1. Panel A. "Cellular interference" mechanism in PCDH19-CE (Modified from [5]). **Panel B.** Interaction of extracellular domains of PCDH19 proteins.

Rare affected males are somatic mosaics carrying postzygotic somatic mutations occurring in some cells of an embryo [5] and show a similar neuropsychiatric profile to females [6], [7]. Transmitting males who can be null for *PCDH19* [8] do not show clinical signs of the disease, which suggests that the function of the protein might be dispensable in the developing brain. With an increasing number of studies on affected males, a new term was proposed for the disease – PCDH19 Clustering Epilepsy (PCDH19-CE) [7], instead of female-restricted epilepsy with ID, which we are using in this manuscript.

PCDH19 protein is a member of the δ2 protocadherin subclass of the cadherin superfamily. *PCDH19* encodes protocadherin 19 protein, which is a cell adhesion molecule. The gene contains six (NM 001184880) or five (NM 020766, NM 001105243) exons where the first one is the largest (2.146 bp) and which encodes six extracellular domains of the protein. (**Figure 1B**).

Gene editing in PCDH19-CE

Nowadays, there is no available permanent therapeutic regimen to cure PCDH19-CE. Epilepsy in PCDH19-CE is often pharmacoresistant and assessment of the existing antiepileptic drugs (AEDs) is difficult because of a possible age-dependent spontaneous seizure remission and provocation of seizure clusters by fever and infection [9], [10]. Antiepileptic drugs such as clobazam, bromide or levetiracetam have shown to be efficient against seizures in 40-70% females for up to 12 months but with the reduction of response during the long-term follow-up [10], [11]. It remains extremely difficult to prevent and abort clustering seizures and, despite the trials of multiple AEDs, patients often require recurrent hospitalisations [12]. Some girls may outgrow seizures naturally but they continue to present ID traits. Therefore, it is important to identify novel therapeutic strategies.

A possible permanent solution to rescue the phenotype can be reached by eliminating all copies of *PCDH19* gene, thus creating a homogenous population on PCDH19 negative cells, recapitulating the situation in transmitting asymptomatic males [8]. To achieve this aim, it is possible to use CRISPR/Cas9 technology to efficiently delete the *PCDH19* gene and abolish the translation of the protein. The CRISPR/Cas9 system, (Clustered Regularly Interspaced Short Palindromic Repeats), is an adaptive defense

system of bacteria against invading viruses. Cas9 gene encodes a CRISPR-associated nuclease type 9 that can mediate capture and cleavage of DNA, guided by single guide RNAs (sgRNAs) [13]. CRISPR/Cas9 technology is widely used to correct disease-causing variants [14–16]. In some cases, genetic therapy employing CRISPR/Cas9 technology is already used successfully in patients [17–19]. To create a deletion of PCDH19 gene, a precise and efficient genetic modification can be achieved by creating two double strand breaks (**Figure 2**) at the locus, allowing the deletion of the intervening DNA segment with subsequent non-homologous end joining (NHEJ) repair [20-24].

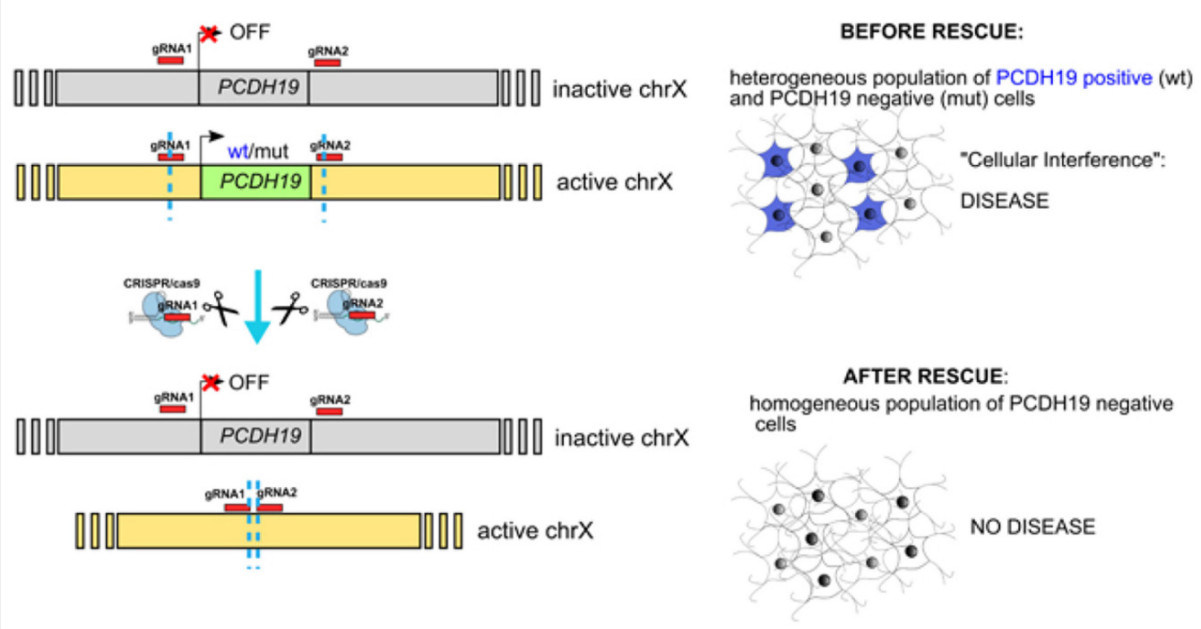

Figure 2. CRISPR/Cas9-mediated PCDH19 deletion.

Modeling PCDH19-CE *in vitro*

Studies of neuronal functions in human diseases are limited by the difficulties to obtain patients' cells from the central nervous system (CNS). For this reason, researchers employ murine models to study PCDH19-CE which allow them to explore the disease mechanisms in the living organism. In particular, studies on murine model showed that protocadherin 19 is highly expressed during development and it is supposed to mediate cell-cell interaction within neuronal circuits and to be involved in neuronal migration

or establishment of synaptic connections [1], [2]. In murine hippocampus, PCDH19 was shown to determine the function of γ-Aminobutyric acid type A receptor (GABAaR) which is a major inhibitory neurotransmitter receptor and ligand-gated ion channel. It was also shown to be a critical determinant of GABAaR-mediated tonic transmission and GABAaR gating causing PCDH19-related hyperexcitability [24]. Some studies of the use of neuronal cells, obtained from murine models, as well provide a great insight into pathophysiology of the disease. It was shown that mosaic expression of *PCDH19* disrupts physiological neurite communication and leads to abnormal neuronal activity in cultured murine neurons [25]. *PCDH19* downregulation reduces GABAaR surface in cultured rat hippocampal neurons [26], and the gene is expressed both in inhibitory and in excitatory neurons, colocalizing partially both with postsynaptic density protein 95 of excitatory neurons (PSD95) and α1-GABAaR subunit [27]. Overall, recent findings on murine models and cells provide a great insight into understanding of the underlying mechanisms of PCDH19-CE.

Human induced pluripotent stem cells (hiPSC) technologies have made it possible to study human neurons and explore physiopathology *in vitro* [28-30]. HiPSC-derived neurons represent a unique opportunity to study neurological diseases of genetic origin, as they maintain the patient's genetics, which is important in the onset and progression of disease [31]. Several studies employed neuronal differentiation from hiPSC to model PCDH19-CE *in vitro*, accurately recreating the mosaic situation in the human brain and showing some prominent results on the maturation, excitability and morphology of human neurons [32-34]. Based on these results, we aimed to differentiate patients' hiPSC into mature neurons, representing mosaic condition of PCDH19-CE (**Figure 3)**, choosing as a differentiation method an overexpression of the transcription factor Neurogenin 2, which will be discussed in details in methods section. Traditional methods of differentiation of hiPSC and embryonic stem cells (ESC) into neurons using commercially available culture and differentiation media are often variable and allow the generation of relatively small amounts of neurons. In addition, it can be quite a long process to generate electrophysiologically active,

mature neurons. Instead, Neurogenin 2-forced differentiation of hiPSCs provides electrophysiologically active neurons in three weeks, characterized by low variability and high reproducibility [35-37].

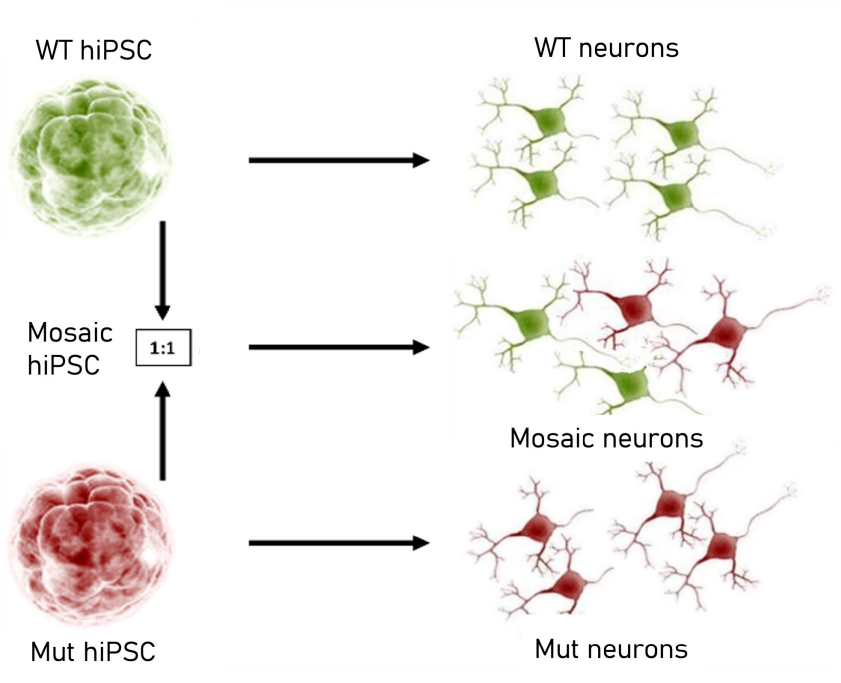

Figure 3. Modeling PCDH19-CE *in vitro.* Clonal hiPSCs derived from patient are mixed in a 1:1 ratio and differentiated in neurons, mimicking the mosaic condition in PCDH19-CE brain.

Aim of the study

The first aim of the study is to create an efficient CRISPR/Cas9 system to introduce a deletion in *PCDH19* gene in cell cultures obtained from affected female patients, and create a knock-out of the gene *in vitro*.

The second aim of the study is to create a PCDH19-CE *in vitro* model through a generation of patient's hiPSC-derived neurons employing an overexpression of the transcriptional factor Neurogenin 2 and assess the morphological and electrical activity properties of neurons.

Material and methods

Study subject and sample collection

A 19-year-old female patient was diagnosed with PCDH19-CE at the Medical Genetics Unit of the Azienda Ospedaliero-Universitaria Senese (Siena, Italy) after Sanger sequencing of *PCDH19* gene. Previously she was tested for the mutations in the *SCN1A* gene – the most common gene causing epilepsy [2] and resulted negative. Genomic DNA of the patient was isolated from EDTA peripheral blood samples using a QIAamp DNA Blood Kit according to the manufacturer's protocol (Qiagen, Germany). The frameshift mutation c.2133delG (p.Thr712Pro) was revealed in the blood cells genomic DNA. The mutation is not yet reported in the literature. The patient has focal epilepsy, mild intellectual disability, mental retardation and motor deficits.

A skin specimen containing epidermis, dermis, and superficial fat was obtained from a punch biopsy of the forearm under local anesthesia. The sample was stored in phosphate buffered saline (PBS) at room temperature (RT) and processed shortly after collection. The study protocol was approved by the Institutional Ethics Committee of the University of Siena / Azienda Ospedaliero-Universitaria Senese, Siena, Italy. The patient (and/or her parents) provided and signed a written informed consent at the Medical Genetics Unit for clinical data usage, and the use of DNA samples for both research and diagnosis purposes.

Cell cultures

All types of cells were cultured in the CO_2 incubator (37 °C, 95% humidity and 5% CO_2, Heracell, Thermo Fisher Scientific, USA). Skin biopsy material from the patient was cut with a sterile blade into pieces of 1-2 mm and put onto 60 mm culture dishes without medium – we let them sit for 5-10 minutes to air dry and attach to the surface and then added 5 ml of complete CHANG Medium C (Irvine Scientific, FUJIFILM, USA). Then the pieces were put into a complete medium for the expansion of fibroblasts. Medium was changed every day until cells started to proliferate and reached 80% confluence. After 5 days in culture cells started to proliferate and we changed medium every other day until they reached 80%

confluence and were routinely passed 1:2 in T-25 or T-75 flasks (Thermo Fisher Scientific, USA) with Trypsin-EDTA 1X (Biowest, France). HEK293T cells were cultured in a complete Dulbecco's Modified Eagle Medium (DMEM) (Thermo Fisher Scientific, USA). Primary rat astrocytes were cultured in a complete Dulbecco's Modified Eagle Medium (DMEM) (Thermo Fisher Scientific, USA).

HiPSCs were cultured on Geltrex LDEV-Free Reduced Growth Factor Basement Membrane Matrix (Thermo Fisher Scientific, USA) coated 6-well and 12-well plates (Thermo Fisher Scientific, USA) in complete StemFlex medium (Thermo Fisher Scientific, USA) with 1% Penicillin-Streptomycin (Thermo Fisher Scientific, USA). Medium was changed every other day. For passaging of cells as cell clumps we incubated them with the Versene Solution 1X (Thermo Fisher Scientific, USA) or 0,5mM Ethylenediaminetetraacetic acid (EDTA) in PBS at room temperature (RT) until the holes in colonies appear, then aspirated the enzymatic solution, collected cell clumps with complete medium and centrifuged for 4 min at 200g. Cell aggregates were then resuspended in complete medium and plated as cell aggregates on Geltrex-coated plates. We cryopreserved cells as described below. For thawing cells, cryovials were prewarmed in a water bath at 37°C until the small icicle remained, resuspended in three volumes of complete medium and centrifuged for four minutes at 200g. To increase cell viability after thawing, we supplemented complete medium with 1% rho kinase (ROCK) inhibitor RevitaCell Supplement (Thermo Fisher Scientific, USA) and replaced it with complete medium after 24h.

Mature neurons were maintained in Neurobasal complete medium (Thermo Fisher Scientific, USA) supplemented with B27 and GlutaMAX (Thermo Fisher Scientific, USA) and containing Brain Derived Neurotrophic Factor (BDNF, 10 ng/ml).

All primary cells and cell cultures were grown in medium with 1% Penicillin-Streptomycin (10,000 U/ml, Thermo Fisher Scientific, USA) unless while being transfected. For cryopreservation, cells were pelleted, resuspended in 1 ml of Fetal Bovine Serum (FBS) (Thermo Fisher Scientific, USA) with 10%

Dimethyl sulfoxide (DMSO) (Sigma, Germany), frozen at -80 °C for 24h and then transferred in a liquid nitrogen tank for longer storage.

Transfection of cells

HEK293T cells were transiently transfected using Lipofectamine 2000 Transfection Reagent 1 µg/µl (Thermo Fisher Scientific, USA) according to the manufacturer's protocol. Fibroblasts were electroporated in suspension using the Neon® Transfection System following manufacturer's protocol (Thermo Fisher Scientific, USA). Number of cells used in electroporation experiments with relative conditions are presented in **Table 1**. Flow cytometry was performed 48 h after transfection. The percentage of enhanced Green Fluorescent Protein (eGFP)-positive cells was quantified with a BD LSRFortessa™ Cell Analyzer (BD Biosciences, USA) cytometer with blue (488 nm) laser, using a 530/30 (eGFP) filter.

Table 1. Conditions of the transfection of fibroblasts with Neon® Transfection System and of the HEK293T cells with Lipofectamine 2000 Transfection Reagent.

Cell type	Cell ɒer	DNA quantity	Conditions
Fibroblasts	$4*10^5$	1) 6-12 µg pLenti_CMV_SaCas9_2U6_2sgRNA_CMV_reporter 2) 3 µg pAAV_2U6_2sgRNA_CMV_eGFP_T2A_Puro (A) + 3 µg pAAV_CMV_SaCas9_HA-tag 3) 3 µg pAAV_CMV_eGFP (control plasmid) 4) 3 µg pAAV empty	1700 V, 1 Pulse, pulse width
HEK293T	$5*10^5$	1) 1 µg pLenti_CMV_SaCas9_2U6_2sgRNA_CMV_reporter 2) 500 ng AAV_2U6_2sgRNA_CMV_eGFP_T2A_Puro (A) ng pAAV_CMV_SaCas9_HA-tag 3) 1 µg pAAV_CMV_eGFP (control plasmid)	Lipofectamine 2000 fection Reagent ɯl

Cellular DNA, RNA and protein isolation

Genomic DNA, total RNA and proteins were isolated from pelleted cells. DNA from cells was extracted using QIAmp DNA Mini Kit (Qiagen, Germany). Total cellular RNA was extracted using TRIzol Reagent and RNeasy mini Kit (Life Technologies, Thermo Fisher Scientific, USA). RNA concentration was quantified using the Nanodrop-1000 spectrophotometer (Thermo Fisher Scientific, USA). Only samples of DNA with 260/280 ratio of 1,8-2,0 and RNA with 260/230 ratio of 2,0-2,2 were used for subsequent analyses. cDNA was synthesized starting from 500 ng of total RNA with QuantiTect Reverse Transcription Kit (Qiagen, Germany) according to manufacturer's protocol. Proteins were isolated with 10-fold excess of Radioimmunoprecipitation assay (RIPA) buffer (Tris-HCL 50mM, NP-40 1%, Na-Deoxycholate 0,5%, SDS 0,1%, NaCl 150mm, EDTA 2mM, pH=7,4) with addition of protease inhibitor cocktail (Sigma, Germany). Protein concentration was quantified with Quantum Protein kit (Euroclone, Italy) using an Agilent BioTek Epoch Microplate Spectrophotometer (Agilent Technologies, USA).

Sanger sequencing

To confirm the presence in the studied cells of the mutation identified in patients' blood cells by the time of the diagnosis we performed Sanger sequencing. Genomic DNA isolated from human primary dermal fibroblasts was amplified by PCR with primers flanking the mutation site (GGGCTCTGTGAACTTGTCCT; CAGAGGAGAAAGTGAGCCTA). Primers were designed using online tool Primer3web version 4.1.0 [38]. PCR products were purified with Agencourt AMPure XP magnetic beads (Beckman Coulter, USA) and loaded for sequencing reaction with BigDye Terminator v3.1 Cycle Sequencing Kit (Thermo Fisher Scientific, Waltham, USA) according to manufacturer's protocol. Samples were precipitated with EtOH/$MgCl_2$, diluted in 24 µl of Formamide (Thermo Fisher Scientific, USA) and loaded on ABI PRISM 3130 Genetic Analyzer (Applied Biosystems, USA).

X-inactivation analysis

X-inactivation analysis was performed on genomic DNA template by standard human androgen receptor (HUMARA) X-chromosome inactivation assay as described in [39] using a forward primer labeled with a fluorescent dye (5'-FAM) GCTGTGAAGGTTGCTGTTCCTCAT and reverse primer TCCAGAATCTGTTCCAGAGCGTGC. Samples were loaded with 0,25 µl of GeneScan 500 LIZ dye Size Standard (Thermo Fisher Scientific, USA) on ABI PRISM 3130 Genetic Analyzer (Applied Biosystems, Thermo Fisher Scientific; USA). To analyze *PCDH19* expression in patients' cells, cDNA was amplified with the same primers used for genomic amplification as they were designed on two different exons and flanking mutation site and sequenced on ABI PRISM 3130 Genetic Analyzer (Applied Biosystems, Thermo Fisher Scientific, USA) as described before.

Next Generation Sequencing

For library preparation we used Ion Ampliseq 2.0 Library Kit (Life technologies, Thermo Fisher Scientific, USA). Libraries were purified with Agencourt AMPure XP magnetic beads (Beckman Coulter, USA) and quantified using Qubit dsDNA HS Assay Kit (Invitrogen, Thermo Fisher Scientific, USA). Libraries were then pooled at equimolar ratio, annealed to carrier spheres (IonSphere Particles, Life Technologies, Thermo Fisher Scientific, USA) and clonally amplified by emulsion PCR (emPCR) on the IonChef System (Ion Chef, Life Technologies, Thermo Fisher Scientific, USA) using the Ion S5 Sequencing Kit. FASTQ files for sequences of DNA from transfected cells and relative controls were analyzed using Integrative Genomics Viewer (IGV) (Broad Institute, USA).

Western blotting

The protein samples (35 µg) were separated by electrophoresis on a polyacrylamide gel (Bolt 4-12% Bis-Tris Plus Gel, Invitrogen, Thermo Fisher Scientific, USA) and then transferred to a nitrocellulose membrane (Invitrogen, Thermo Fisher Scientific, USA) using the iBlot 2 Gel Transfer Device (Invitrogen,

Thermo Fisher Scientific, USA). Membranes were incubated in blocking solution – 5% milk solution in Tris-buffered saline 1X (TBS) with 0,1% Tween 20 (Promega, USA) – for 1h at RT, and then with mouse anti-HA-tag antibody (1:1000, 18181, Abcam, UK) and mouse anti-β-Actin (C4): (1:1000, sc-47778, Santa Cruz Biotechnology, USA) overnight at 4°C. Membranes were incubated for 1h at RT with a horse-radish peroxidase (HRP)-conjugated rabbit anti-mouse IgG (1:1000) and incubated with the commercial kit solution SuperSignal West Pico PLUS Chemiluminescent Substrate (Thermo Fisher Scientific, USA). The membranes were developed with ChemiDoc XRS+ (Bio-Rad, USA).

Generation of hiPSCs and hiPSC-derived neurons

PCDH19-mutated hiPSC clones used in the study were generated and characterized by Marina Cardano from the Cell Technology Facility (CIBIO – University of Trento). HiPSC clones were obtained from patient's skin fibroblasts using Sendai virus particles delivering Yamanaka factors (CytoTune-iPS 2.0 Sendai Reprogramming Kit, Thermo Fisher Scientific, USA). $4*10^5$ cells were transduced with 16 µl cMYC virus, 13,5 µl KOS virus and 9 µl KLF4 virus at the appropriate MOI according to manufacturer's protocol. After reprogramming, the hiPS cells were characterized by immunostaining and was performed Embryoid Body (EBs) trilineage assay. EBs are three-dimensional aggregates of three germ layer cells. Through the formation of EBs we confirmed the ability of hiPSCs to differentiate into each of the three germ layers.

Mature neurons were obtained from hiPSC through the overexpression of transcription factor Neurogenin 2 (Ngn2) by infection with lentiviral vectors to stably integrate transgenes into the genome of hiPSCs (**Figure 4A**). The major part of the induced neurons obtained with this protocol are excitatory and the protocol was modified from [35-37].

Briefly, we produced ultra-concentrated Lentivirus encoding Ngn2 and rtTA plasmids (a gift from Prof. Anna Margherita Corradi, Department of Experimental medicine, University of Genoa) using calcium phosphate method of transfection with third generation lentiviral packaging vectors (Addgene plasmids #12251, #12253, #182229) in HEK293T cells [40]. RtTA virus encodes a Tet-On Advanced transactivator

and the second virus encodes Ngn2 under the control of Tet-controlled promoter, GFP cassette and blasticidin resistance gene (BSD) as a fusion protein linked by P2A and T2A sequences (**Figure 4B**).

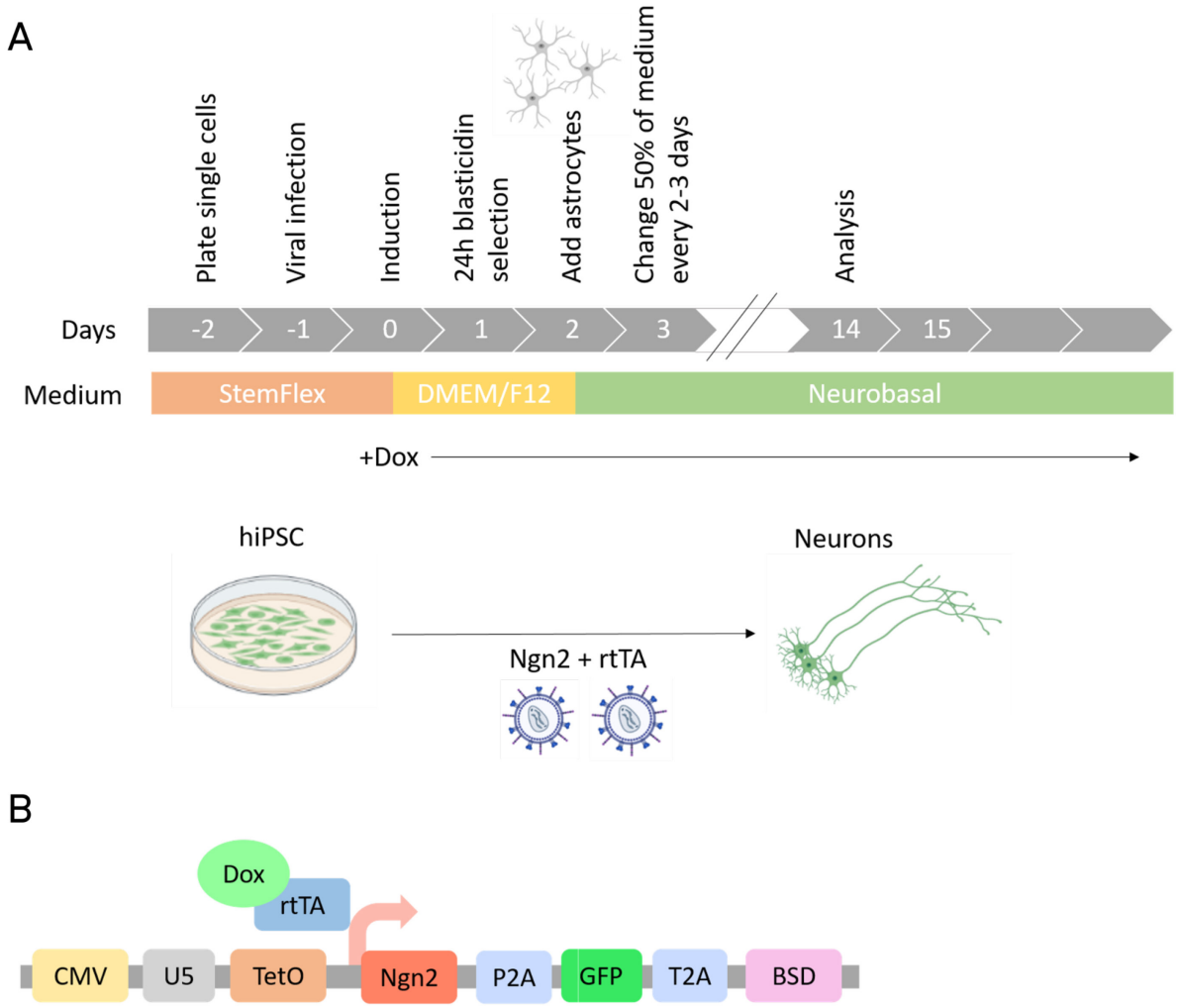

Figure 4. Generation of rtTA/Ngn2 positive hIPSCs. **Panel A.** Differentiation workflow. **Panel B.** Schematic of induction system. Cells are infected with a virus expressing Ngn2/GFP/Blasticidin resistance gene as a fusion protein and rtTA-expressing virus.

On day −2, feeder-free hiPSCs were treated with Accutase (StemCell Technologies, Canada) and plated as dissociated cells on Poly-L-Ornithine (50 µg/ml, Sigma, Germany) / Laminin (10 µg/ml, Sigma, Germany) - coated 12mm coverslips as described in [14]. Cells were seeded at the density 50.000 cells/well in a 24-well plate in complete StemFlex medium (Thermo Fisher Scientific, USA). ROCK inhibitor

(Y27632, 2 µM, StemCell Technologies, Canada) was added to StemFlex medium to increase cell viability. On day -1, cells were infected with Ngn2 and rtTA lentiviruses at concentration MOI=5 per well in StemFlex medium and incubated overnight with viruses. The day after the medium was replaced by DMEM/F12 supplemented with N2 (1%, Thermo Fisher Scientific, USA), non-essential amino acids (1%, NEAA, Thermo Fisher Scientific, USA), Penicillin-Streptomycin (1%, Thermo Fisher Scientific, USA), human BDNF (10 ng/ml Thermo Fisher Scientific; USA), mouse laminin (0,2 µg/ml, Sigma, Germany) and doxycycline (2 µg/ml, Thermo Fisher Scientific, USA). Doxycycline (2 µg/ml Thermo Fisher Scientific, USA) was added on day 0 to induce TetO gene expression and was maintained until the end of the experiment. On day 1 was added blasticidin (10 µg/ml Thermo Fisher Scientific, USA) and left for 24 hours to select infected cells. On the day postinfection (DPI) 2 we added 50.000 rat astrocytes per well to generate electrophysiologically active neurons. Astrocytes were added in Neurobasal complete medium (Thermo Fisher Scientific, USA) supplemented with B27 and GlutaMAX (Thermo Fisher Scientific, USA) containing BDNF (10 ng/ml). After DPI 2, 50% of the medium in each well was changed every 2-3 days.

Astrocyte isolation and culture

For every experiment, two cortices were obtained from mouse or rat pups dissection. Tissue was digested by 1 ml of Trypsin-EDTA 1X (Thermo Fisher Scientific, USA) for 30 minutes in a water bath at 37°C with occasional shaking every 10 minutes. The tissue was dissociated into a single cell suspension by harsh trituration in three volumes of DMEM medium (Thermo Fisher Scientific, USA) completed with 1% GlutaMAX (Thermo Fisher Scientific, USA) and 10% FBS (Thermo Fisher Scientific, USA) with 1% Penicillin-Streptomycin (Thermo Fisher Scientific, USA) to avoid the growth of neurons. Cells were centrifuged at 1000 rpm for five minutes. Mixed cortical cells were resuspended in 13 ml of complete medium and plated onto T-75 culture flasks (Thermo Fisher Scientific, USA). Medium was changed two days after plating. After 7-8 days, when astrocytes reached confluency and overlaying microglia sat exposed on the astrocyte layer (**Figure 5**), we detached oligodendrocyte precursor cells by hitting the flask against the palm of the hand for five minutes and rinsed the remaining confluent astrocyte layer twice with PBS

(Thermo Fisher Scientific, USA). Astrocytes were then routinely passed one or two times with Trypsin-EDTA 1X (Thermo Fisher Scientific, USA) for expansion before the differentiation experiment. Cells were cryopreserved and thawed as described above.

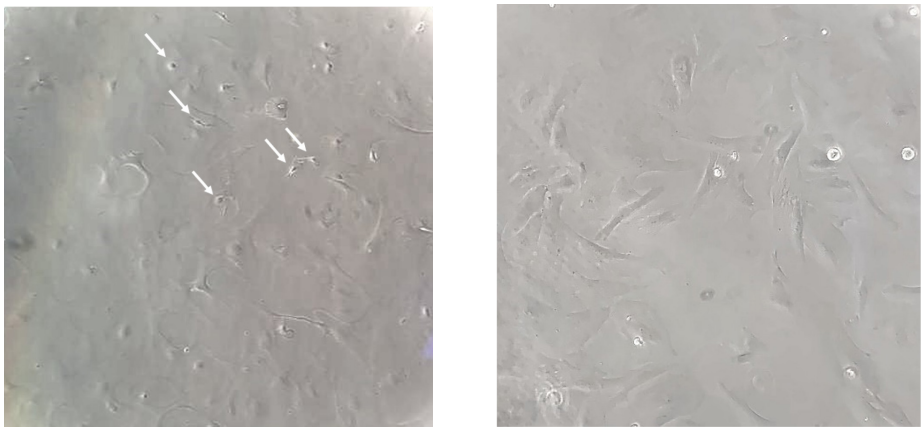

Figure 5. Morphological overview of isolated mixed cortical cells (left) and pure astrocyte culture at DIV 7 and after the first passage (right). Astrocyte layer is completely confluent with microglia and oligodendrocytes on top of an astrocyte layer (white arrows).

Lentivirus production

HiPSC were differentiated in neurons through overexpression of transcription factor Neurogenin 2 (Ngn2) which determines neuronal fate (**Figure 4**). For this aim, we produced ultra-concentrated Lentivirus encoding NGN2 and rTta plasmids using calcium phosphate method of transfection with 3d generation lentiviral plasmids [40] in HEK293T cells.

HEK293T cells were thawed in complete DMEM medium (Thermo Fisher Scientific, USA) as described above one week before the experiment and routinely passed 1:10 with Trypsin-EDTA 1X (Biowest, France) when reached 70-80% confluence. $3*10^6$ cells were plated in 28 sterile 100 mm dishes (Thermo Fisher Scientific, USA). On the next day the medium was changed to complete DMEM with pyruvate (Thermo Fisher Scientific, USA). After 3-4 h we transfected cells with the following constructs:

1. Transfer vector (Ngn2 or rTta): 13 µg/plate;

2. Packaging plasmid (pMDLg/pRRE, (Addgene plasmid #12251; http://n2t.net/addgene:12251; RRID:Addgene_12251)): 13 µg/plate;

3. Second packaging plasmid (pRSV-Rev, (Addgene plasmid #12253; http://n2t.net/addgene:12253; RRID:Addgene_12253)): 3 µg/plate;

4. Envelope plasmid (pMD2.VSVG, (Addgene plasmid #182229; http://n2t.net/addgene:182229; RRID:Addgene_182229)): 3,75 µg/plate.

We prepared a mix of DNA, $CaCl_2$ 2,5M (50µl/plate) and sterile ultrapure water in the final volume of 0,5 ml/plate. Then we added the mix dropwise to 0,5 ml/plate of HBS 2x (500 ml: NaCl 8g, KCl 0,38g, Na_2HPO_4 0,1g, Hepes 5g, Glucose 1g, pH=7,05) bubbling the solution with an automatic pipette attached to a glass Pasteur. The precipitate was left to sit undisturbed for 20 minutes at RT and added dropwise evenly over the cell culture medium on the plate (1 ml/plate). The dishes were gently agitated to distribute the precipitates evenly over the cells on the plate and incubated overnight in the CO_2 incubator (37 °C, 95% humidity and 5% CO_2, Heracell, Thermo Fisher Scientific, USA). Next day the cells were washed in PBS $+Ca^{2+}$ Mg^{2+} (Thermo Fisher Scientific, USA) and the medium was changed to a fresh one. Plates were incubated for 24h for virus production. Medium was filtered with 0,22 µm filters (Millipore), added to plastic tubes containing 4 ml of 20% sucrose in PBS $+Ca^{2+}$ Mg^{2+} (Thermo Fisher Scientific, USA) and centrifuged at 26000 rpm for 1h 30m at 4°C. Supernatant was discarded and pellet was left to dry for 5 minutes. Pellet was left in DPBS $+Ca^{2+}$ Mg^{2+} for 40 min at 4°C, then resuspended in 400 ul of DPBS $+Ca^{2+}$ Mg^{2+} (all tubes) and centrifuged at 23.000 rpm per 1h 30min a 4°C. Pellet was resuspended in 40 µl of DPBS $+Ca^{2+}$ Mg^{2+} and left at 4°C for 1h. The suspension was centrifuged at 7000 rpm for 5 minutes and resuspended in DPBS $+Ca^{2+}$ Mg^{2+} by pipetting around 40 times. Aliquots of 2ul were frozen at -80°C. To determine the titer of the virus, on the day 1, HEK293T cells were plated in 6-well plates at the density of $1*10^5$ cells/well in order to achieve 30-50% confluence on day 2. On the next day, $2,4*10^5$ cells were infected with ten-fold serial dilutions of the lentivirus preparation from $1*10^{-3}$ to $1*10^{-7}$ in 2 ml of complete DMEM medium. Cells were incubated in the CO_2 incubator (37°C, 95% humidity and 5% CO_2, Heracell,

Thermo Fisher Scientific, USA) and monitored under the microscope for the expression of GFP. When the fluorescence was visible (after 72h), cells were detached with Trypsin-EDTA 1X (Biowest, France), centrifuged for 5 min at 1000 rpm, washed in PBS (Thermo Fisher Scientific, USA) and fixed for 15 min in 4% Paraformaldehyde (PFA) at RT. Fixed cells were washed in PBS twice followed by centrifuge for 5 min at 1000 rpm, resuspended in 250 ul of PBS in FACS tubes and stored at 4°C. FACS analysis was performed on Cytoflex flow (Beckman Coulter, USA) cytometer with blue (488 nm) laser, using a 530/30 (GFP) filter in 3-4 days after fixation.

To calculate the functional titer of the lentivirus particles, we chose 1% to 20% GFP-positive (GFP+) populations. Below 1% GFP+, FACS may not reliably determine the number of positive cells; above 20% GFP+, there are high chances for each GFP+ target cell to be transduced twice, resulting in an underestimation of the number of transducing particles [41]. Based on the chosen populations, we calculated a functional titer in transducing units (TU) per ml, using the following formula:

$$TU/ml = (\text{cell count per well} * \% (GFP+ \text{ cells})) / \text{dilution factor}$$

Then we calculated the medium viral titers of chosen population and used this number to establish a volume of virus for iPSC transduction using MOI (Multiplicity of Infection) = 5 according to the following formula:

$$\mu l \text{ (virus)} = (\#\text{cells} * MOI) / \text{viral titer}$$

Coating for cell cultures

For hiPSC cultures, we used Geltrex (Thermo Fisher Scientific, USA) coating. Geltrex was diluted 1:10.000 in cold PBS with Ca+Mg+ (Thermo Fisher Scientific, USA), vortexed and added to multiwell plates, followed by 1h of incubation in humidified 37°C incubator with an atmosphere of 5% CO_2 or overnight at 4°C. For hiPSC-derived neurons was used Poly-L-Ornithine/Laminin coating. Poly-L-Ornithine solution (Sigma, Germany) was diluted in sterile ultrapure water in concentration 50 µg/ml.

Multiwell plates were incubated 2h at RT or overnight at 4°C. Then the solution from plates was aspirated, wells washed twice with sterile ultrapure water followed by third wash with DMEM/F12 basal medium (Thermo Fisher Scientific, USA). Laminin from Engelbreth-Holm-Swarm murine sarcoma basement membrane (Sigma, Germany) was diluted in cold DMEM/F12 to a final concentration of 10 μg/ml. Plates were then incubated 2h at RT or overnight at 4°C.

Immunostaining

HiPSCs and neurons were fixed with 4% Paraformaldehyde (PFA) at RT for 15 min and then permeabilized in 0,1% Triton in PBS (Thermo Fisher Scientific, USA) for 5 min at RT. Cells were blocked for 1h at RT in 5% (hiPSC) or 10% (neurons) FBS in PBS-Triton 0,1%. For hiPSC, primary antibodies were diluted in 3% FBS in PBS-Triton 0,1%: SOX2 (1:200, GTX101507, Genetex, USA), Nanog (1:200, sc-376915, Santa Cruz, USA), FOXA2 (1:100, sc-374376, Santa Cruz, USA), T-Brachyury (1:100, sc-166962, Santa Cruz, USA) and incubated overnight at 4C in humid conditions in the dark. For neurons, primary antibodies were diluted in 5% FBS in PBS-Triton 0,1% at following dilutions: PCDH19 (1:300, HPA001461, Sigma, Germany), NeuN (1:300, ab177487, Abcam, UK), β3-Tubulin (1:300, sc-80005, Santa Cruz, USA) and incubated for 2h at RT in humid conditions in the dark. Incubations with secondary antibodies diluted in 3% or 5% FBS in PBS-Triton 0,1%, for hiPSCs and neurons, respectively, were performed for 1h at RT at following dilutions: goat anti-mouse or anti-rabbit IgG (H+L) Cross-Adsorbed Secondary Antibody, Alexa Fluor 568 (1:2500, A-11004 and A-11011, Invitrogen, USA). Cells were finally incubated with 4′,6-diamidino-2-phenylindole (DAPI) for 5 min at RT in the dark. Coverslips were mounted with Vectashield Antifade Mounting Medium (Vector Labs, USA). Samples were analysed by a confocal laser microscope Leica TCS SP8 (Leica, Germany) with 405 lex and 440–480 lem, 488 lex and 490-540 lem and 561 lex and 578–625 lem for DAPI, GFP and Alexa Fluor 568, respectively. All images were processed using ImageJ software (National Institutes of Health, USA).

Electrophysiology

Whole-cell patch-clamp electrophysiological recordings were performed by Prof. Maria Passafaro and Luca Murru in the NeuroMI Milan Center for Neuroscience, at the University of Milano-Bicocca with a Multiclamp 700B amplifier (Axon CNS Molecular Devices, USA) and using an infrared-differential interference contrast microscope Nikon Eclipse FN1 (Nikon, Japan). Patch electrodes (borosilicate capillaries with a filament and an outer diameter of 1,5 μm; Sutter Instruments, USA) were prepared with a four-step horizontal puller (Sutter Instruments, USA) and had a resistance of 3–5 MΩ. Voltage- and Current-clamp experiments were performed using an intracellular solution containing (in mM): 126 K-gluconate, 4 NaCl, 1 EGTA, 1 $MgSO_4$, 0,5 $CaCl_2$, 3 ATP (magnesium salt), 0.1 GTP (sodium salt), 10 glucose, and 10 HEPES–KOH (pH 7,28), and an external solution containing (in mM) 138 NaCl, 4 KCl, 2 $CaCl_2$, 1.2 $MgCl_2$, 10 HEPES, and 10 D-glucose, adjusted to physiological pH 7,4 with NaOH. To evaluate hiPSC-derived neurons active and passive membrane properties, a series of depolarizing current steps (0–230 pA) were injected (10 pA per step, 0,5 s duration) to evoke action potential (AP) firing. The AP frequency was correlated to the current injected in an input/output (I/O) curve. AP feature analysis was performed for the first AP evoked at rheobase. Voltage-clamp recordings of inward and outward currents were elicited by 5 mV steps (10 ms) from −75 to +85 mV and neurons were held at −65 mV. Currents were amplified, filtered at 5 kHz and digitized at 20 kHz. All the analyses were performed offline with Clampfit 10.1 software (PClamp, Molecular Devices, USA).

Results

CRISPR/Cas9 system design

To create a knock-out of *PCDH19* gene we designed three different pairs of two single guide RNAs (sgRNAs) flanking the ends of the first exon (set (A)), the ends of the first and third exons (set (B)), and the ends of *PCDH19* cDNA (set (C)) (**Table 2; Figure 6C**). Guide RNAs drive the Cas9 nuclease to the target sequences by recognizing adjacent Protospacer Adjacent Motif (PAM) specific for the *Staphylococcus aureus* Cas9 variant (SaCas9): 5'-NNGRRT-3'. SgRNA 1 and 2 sequences (including PAM) are represented in **Table 2**.

Table 2. sgRNA 1°(FW-forward) and 2°(RV-reverse) sequences (including PAM).

sgRNA	**5'-3' sequence**
set (A)_ sgRNA+pam 1°: exon 1 (FW) set (B)_ sgRNA+pam 1°: exon 1 (FW)	(g)AGGCAGAGCCCCGTGCAGCCATGGAG
set (A)_ sgRNA+pam 2°: exon 1 (RV)	TGTCCCCTGCTCTCGATGCCCAAGAGT
set (B)_sgRNA+pam 2°: exon 3 (RV)	ACTCTTTCAACAGCCAGGGGCCCCAGC(g)
set (C)_ sgRNA+pam 1°: out of exon 1 (FW)	GCTAACTTTGAAGGGGTAAAACTGAGT
set (C)_ sgRNA+pam 2°: exon 6 (RV)	ATTCTGAAGGAAGGTCGCAACAAAGAG

The first vector we designed is based on a lentiviral backbone containing SaCas9 coding sequence, two sgRNAs, each one under the control of its own human U6 promoter, and a double reporter system (mCherry and eGFP) under the control of CMV promoter. The additional target sequence for Cas9 + PAM

connects together the mCherry and the eGFP out-of-frame sequence. In this way, mCherry is expressed constitutively once the plasmid enters the cell and eGFP returns into the coding frame only when Cas9 cuts the target sequence, thus allowing us to select the edited eGFP expressing cells (**Figure 6A**). We cloned three different pairs of sgRNAs (**Table 2**) in lentiviral plasmids to assess their efficiency.

The second vector system is based on two adeno-associated viral backbone plasmids. One plasmid contains SaCas9 conjugated with an epitope tag (HA-tag) under the control of CMV promoter and the other plasmid encodes two sgRNAs each one under the control of its own human U6 promoter, CMV promoter driving expression of eGFP and puromycin resistance cassette for selection of transfected cells (**Figure 6B**). In the case of AAV vectors, eGFP positivity represents successfully transfected cells. In the following experiments, we used letters A, B, and C to indicate which sgRNA pair was inserted into the vectors.

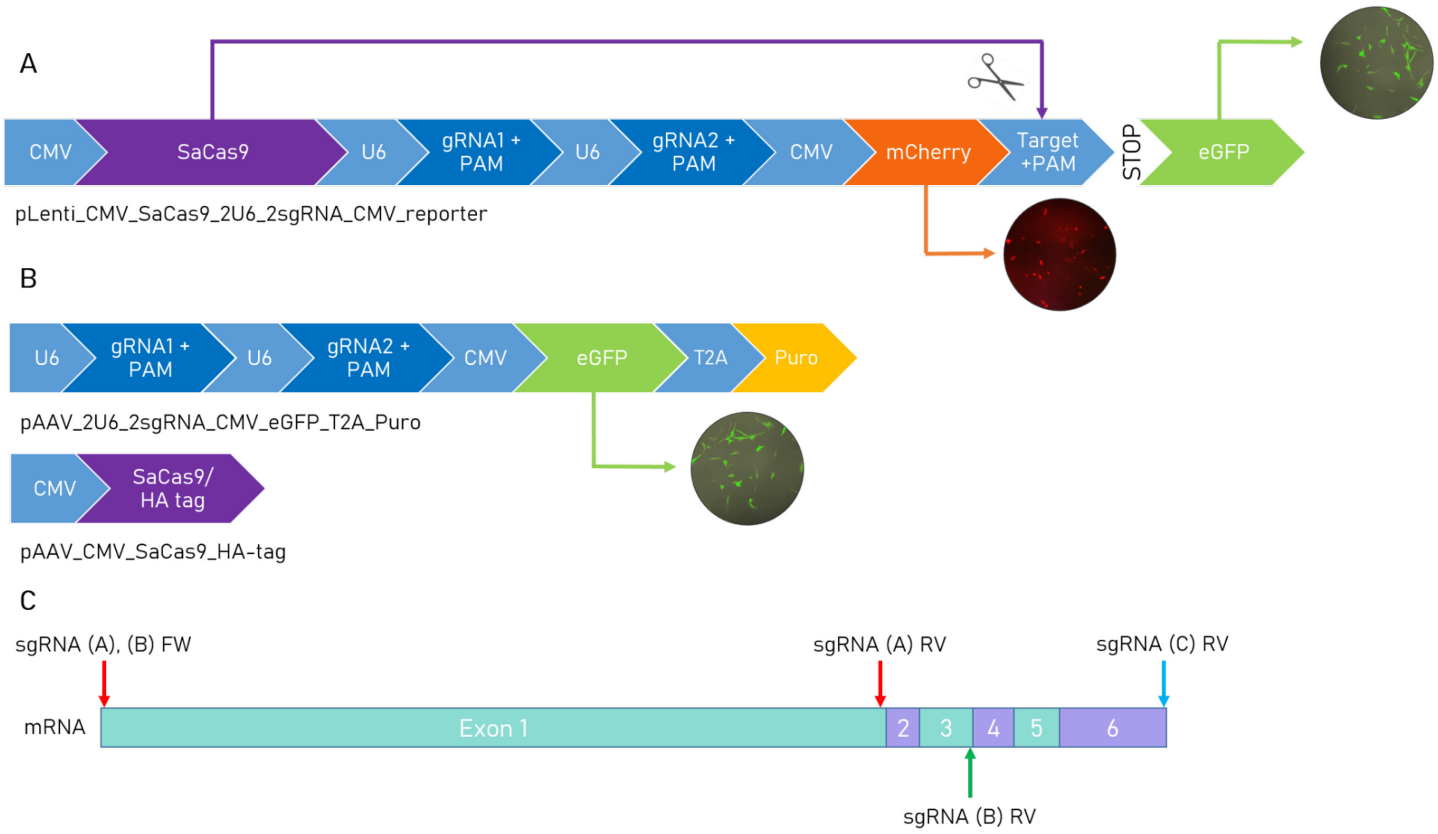

Figure 6. Panel A. Schematic of pLenti_CMV_SaCas9_2U6_2sgRNA_CMV_reporter vector. Following the recognition of target sequence + PAM by SaCas9, eGFP sequence returns in the coding frame and cells express eGFP protein. **Panel B.** Schematic of pAAV_2U6_2sgRNA_CMV_eGFP_T2A_Puro and pAAV_CMV_SaCas9_HA-tag vector. Two co-transfected plasmids allow SaCas9 from one vector and gRNAs+PAM from another to recognise and cut target sites. **Panel C.** Position of sgRNAs pairs on the *PCDH19* mRNA.

SgRNA efficiency test and application of lentivirus-based vectors in patients' cells

Firstly, we checked the efficiency of transfection of HEK293T cells with pLenti_CMV_SaCas9_2U6_2sgRNA_CMV_reporter carrying different sgRNA pairs (A), (B) and (C) (**Table 2**) using Lipofectamine 2000 reagent (Thermo Fisher Scientific, USA). We assessed the transfection efficiency of these vectors by FACS (**Figure 7**). The lentiviral vectors with double reporter (**Figure 6A**) and different sgRNA pairs showed the following percentages of double positive (eGFP+ and mCherry+) cells **(Figure 7, UR quadrant)**: (A) showed 64,63%, (B) – 29,92%, and (C) – 87,03%. At the same time, (A) and (B) resulted in 18,35% and 23% of mCherry+ cells **(Figure 7, UL quadrant)**, while (C) showed only 1%. With double reporter, mCherry is expressed constitutively and its expression together with the absence of eGFP expression means that in these cells plasmid has only entered the cells but SaCas9 is not expressed. Therefore, the pLenti_CMV_SaCas9_2U6_2sgRNA_CMV_reporter (C) that has shown 87,03% of double positive (eGFP+ and mCherry+) cells and only 1% of mCherry+ cells has the highest efficiency of transfection.

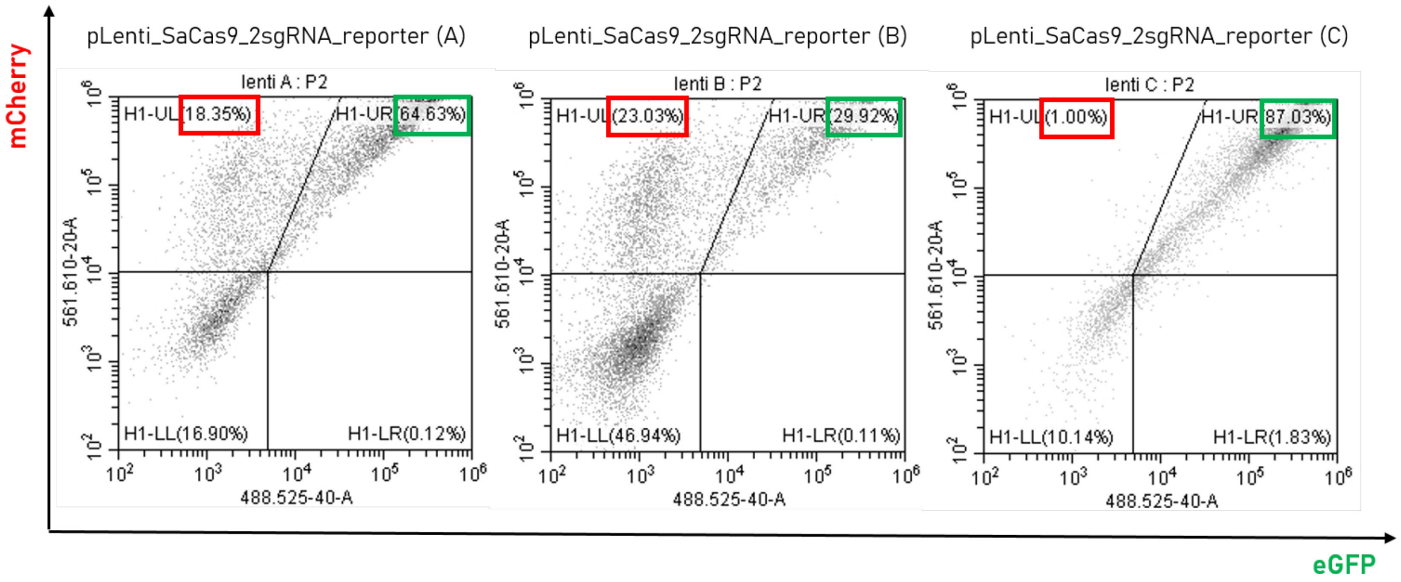

Figure 7. Transfection of HEK293T cells with pLenti_CMV_SaCas9_2U6_2sgRNA_ CMV_reporter carrying different sgRNA pairs (A), (B) and (C). On the X axis – eGFP expression; on the Y axis – mCherry expression. In the upper left quadrant (UL) are represented mCherry+ cells, in the upper right quadrant (UR) – double positive (eGFP+ and mCherry+) cells, lower left quadrant (LL) – non-transfected cells, lower right quadrant (LR) – eGFP+ cells.

Given the different efficiency of transfection in HEK293T cells, we electroporated the fibroblasts with the lentiviral plasmids containing sgRNAs (A) and (C) and consequently assessed the percentage of eGFP-positive cells. In case of double reporter, eGFP positivity indicates editing events performed by the SaCas9 nuclease. The percentage of eGFP-positive cells transfected with pLenti_CMV_SaCas9_2U6_2sgRNA_CMV_reporter (A) was 20,5% (Figure 3A, P1 gate) and with pLenti_CMV_SaCas9_2U6_2sgRNA_CMV_reporter (C) – 48,5% (Figure 3B, P3 gate) in comparison with control transfection with the vector expressing only eGFP (pAAV_CMV_eGFP), which resulted in 94,1% and 92,9%, respectively. In the case of pLenti_CMV_SaCas9_2U6_2sgRNA_CMV_reporter (A) we also observed the changes in the morphology of the cells which appeared as two separate populations (**Figure 8A**, P2 and P3 gates).

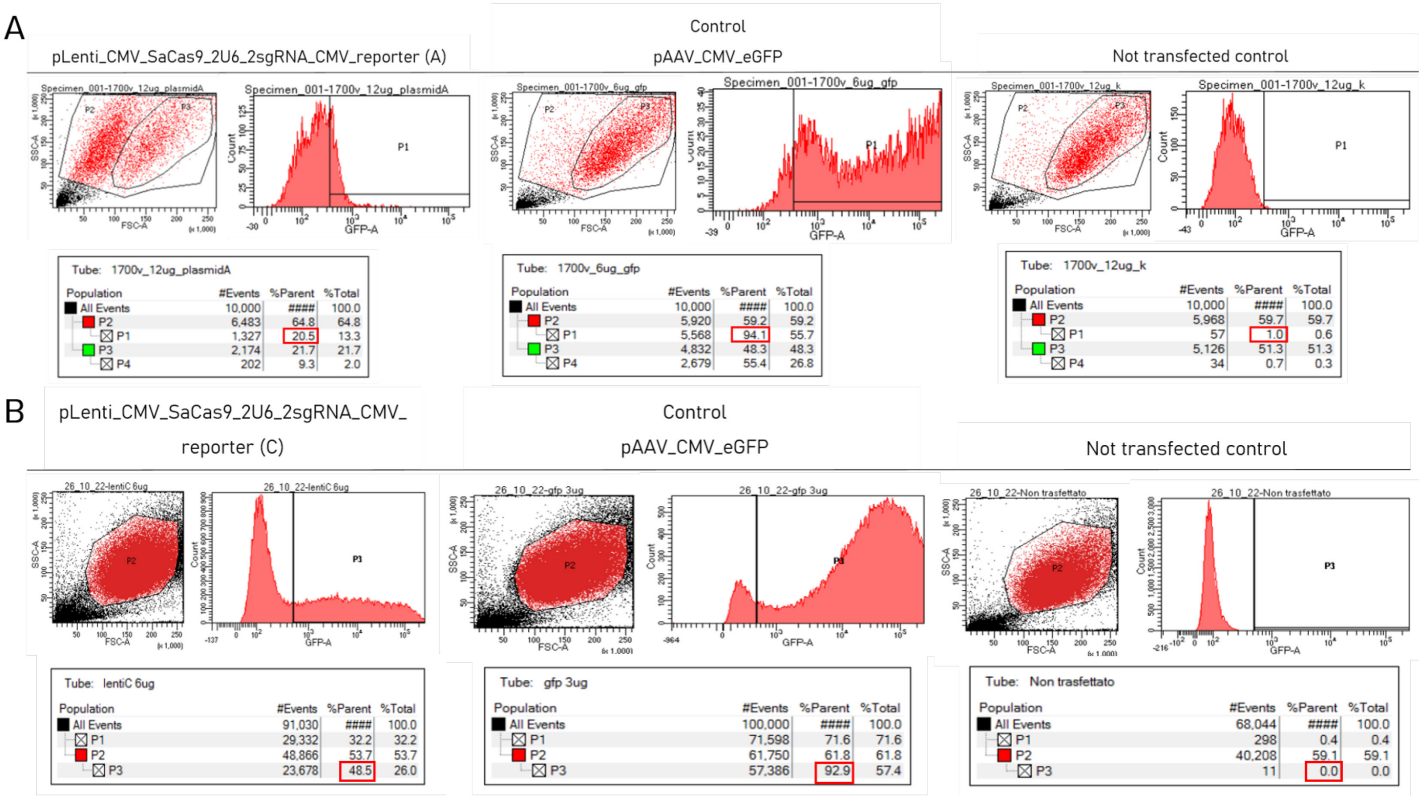

Figure 8. Representative plots of transfection in fibroblasts. **Panel A.** Transfection with pLenti_CMV_SaCas9_2U6_2sgRNA_CMV_reporter (A), control vector pAAV_CMV_eGFP and non-transfected control fibroblasts from the same patient. Gate P2 – all live cells; gate P1 – eGFP+ cells. **Panel B.** Transfection with pLenti_CMV_SaCas9_2U6_2sgRNA_CMV_reporter (C), control vector pAAV_CMV_eGFP and non-transfected control fibroblasts from the same patient. Gate P2 – all live cells; gate P3 – eGFP+ cells.

Application of AAV-based vectors in patients' cells

Given the comparatively high specificity of the sgRNA pair (A) and its low efficiency using the lentiviral plasmid with the double reporter, we cloned the sgRNA pair (A) in a vector based on the AAV backbone with only eGFP reporter (**Figure 6B**). To test the plasmid functionality, we transfected HEK293T cells with pAAV_2U6_2sgRNA_CMV_eGFP_T2A_Puro (A) and pAAV_CMV_SaCas9_HA-tag and confirmed the efficiency of transfection by visual examination (**Figure 9A**) and Western Blotting of lysates of transfected and non-transfected HEK293T cells (**Figure 9B**), showing the presence of HA-tag conjugated with SaCas9 inside the transfected cells.

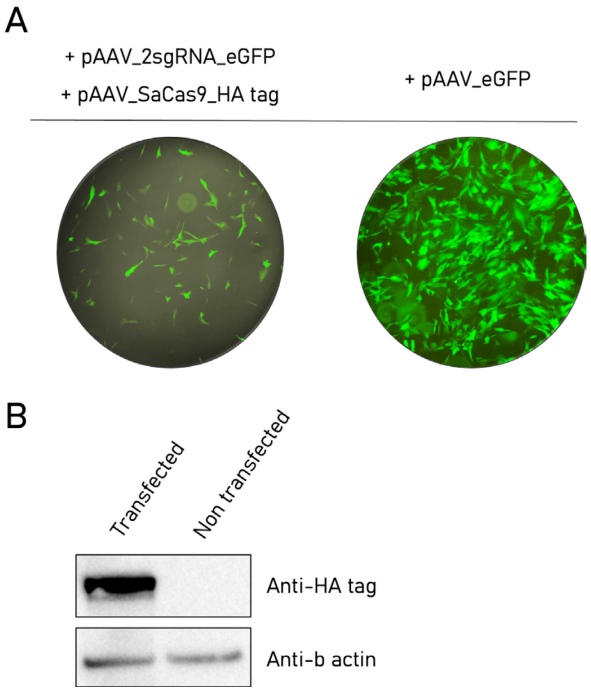

Figure 9. Panel A. eGFP expression in HEK293T cells transfected with pAAV_2U6_2sgRNA_CMV_eGFP_T2A_Puro (A) and pAAV_CMV_SaCas9_HA-tag and control HEK293T cells transfected with pAAV_CMV_eGFP. **Panel B.** Representative western blot of lysates of transfected HEK293T cells. The expression of HA-tag conjugated SaCas9 in transfected HEK293T cells and the absence of its expression in the non-transfected control.

We co-transfected the fibroblasts with pAAV_2U6_2sgRNA_CMV_eGFP_T2A_Puro (A) and pAAV_CMV_SaCas9_HA-tag and selected them with puromycin (Merck, Germany) in concentration 1 ug/ml. The transfection resulted in 72,9% of eGFP-positive cells (**Figure 10A**, gate P3), which in this case indicated the transfection efficiency. As the control transfection vector, we used pAAV_CMV_eGFP together with empty pAAV plasmid, which resulted in 91,7% of eGFP+ cells. We sequenced bulk DNA from fibroblasts transfected with pAAV_2U6_2sgRNA_CMV_eGFP_T2A_Puro (A) together with pAAV_CMV_SaCas9_HA-tag and non-transfected fibroblasts and observed a decrease of 46,1% and 59,5% in the number of reads in transfected sample in the regions targeted by sgRNA1 and sgRNA2, respectively, comparing to control (**Figure 10B**).

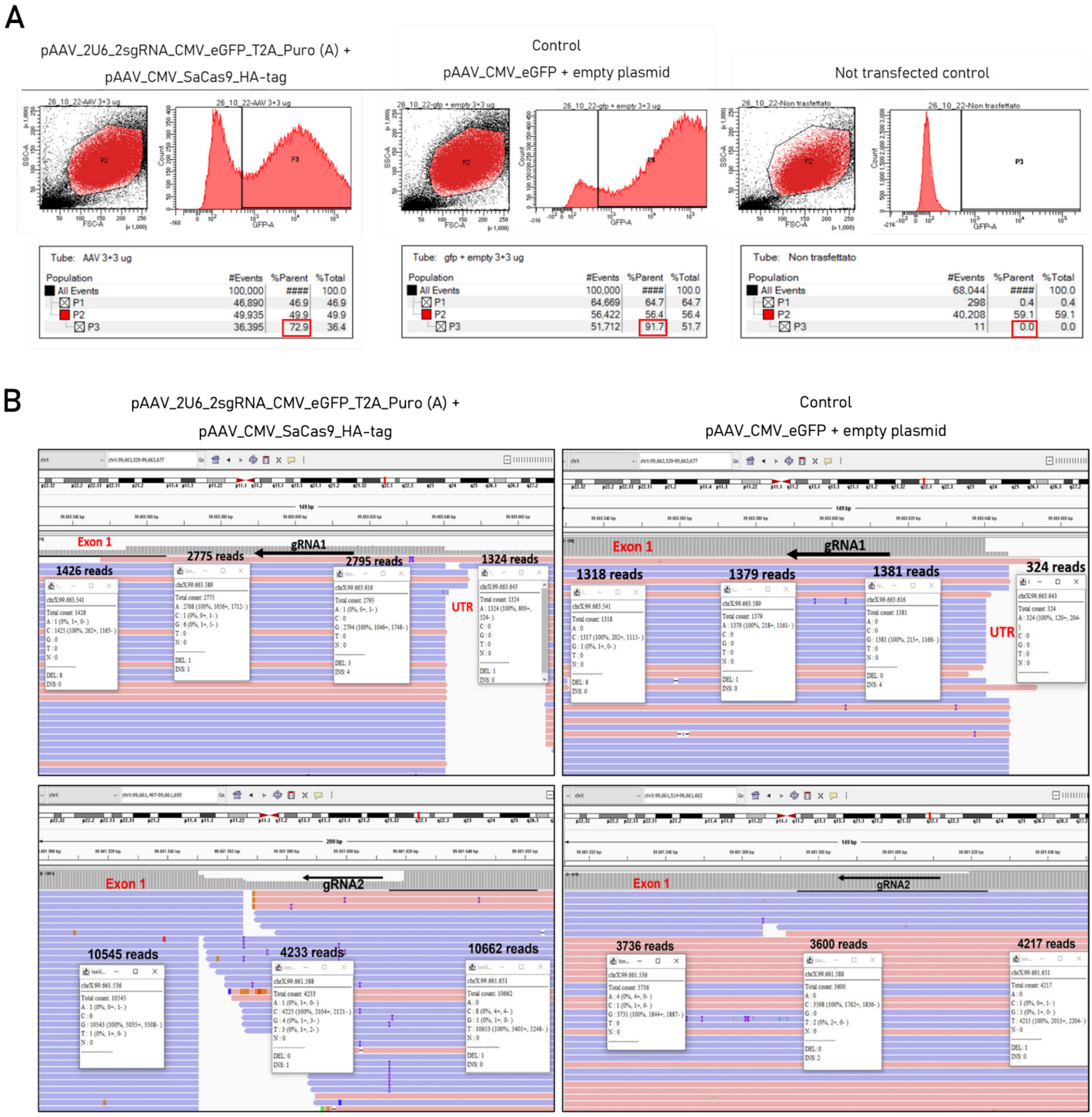

Figure 10. Panel A. Transfection with pAAV_2U6_2sgRNA_CMV_eGFP_T2A_Puro (A) together with pAAV_CMV_SaCas9_HA-tag, pAAV_CMV_eGFP together with empty pAAV plasmid, and non-transfected control fibroblasts from the same patient. Gate P2 – all live cells; gate P3 – eGFP+ cells. **Panel B.** Next-Generation Sequencing results in fibroblasts transfected with pAAV_2U6_2sgRNA_CMV_eGFP_T2A_Puro (A) together with pAAV_CMV_SaCas9_HA-tag (bulk DNA) and non-transfected fibroblasts (control).

PCDH19 expression in hiPSC clones and characterisation

Patient's skin fibroblasts were analyzed for X-inactivation and a skewed X-inactivation pattern was confirmed by a HUMARA assay and showed a ratio of 75:25 (data not shown). Sanger sequencing of cDNA from fibroblasts confirmed the expression of both WT and mutated alleles (**Figure 11A**). cDNA sequencing of the two hiPSC clones obtained from the patient's skin fibroblasts revealed clonal expression of either mutant or WT allele (**Figure 11B**). The mechanism of the changes in X-inactivation occuring during reprogramming of cells coming from female cell lines will be explained below in the Discussion section. To create a cell model of PCDH19-CE where both cell populations co-exist, we mixed WT and mut hiPSC clones in a ratio 1:1, thus obtaining ("mosaic" hiPSCs), where part of the cells WT allele and part – mutated allele. The sequencing of the bulk cDNA of mosaic hiPSCs confirmed the presence of two overlapping sequences after the mutation site, created by the presence of both WT and mut sequences from two cell populations (**Figure 11B**). The cells carrying the WT allele of *PCDH19* gene were used as control.

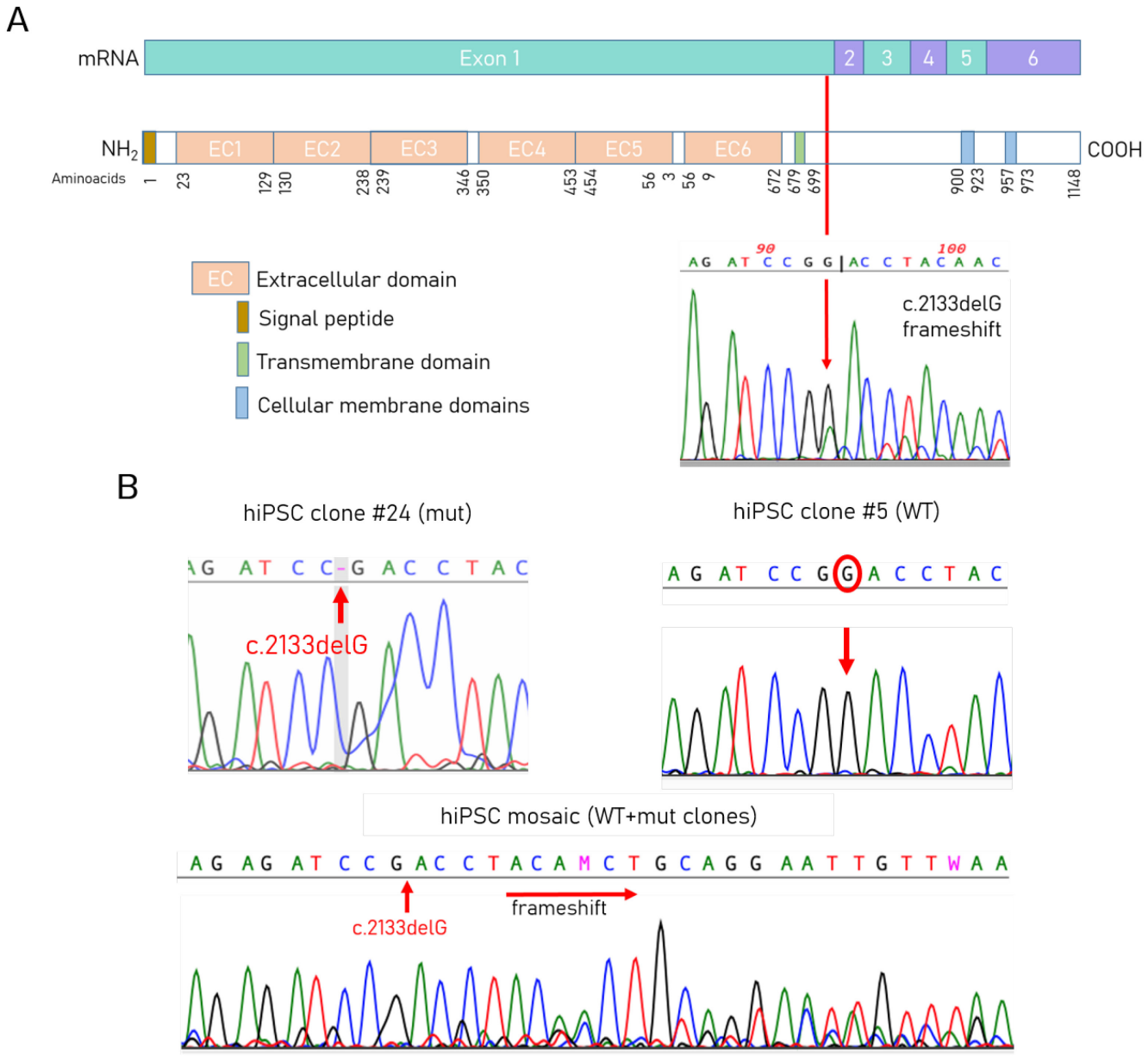

Figure 11. **Panel A.** Sequence of cDNA from patients' fibroblasts and its position on the map of PCDH19 mRNA and protein. **Panel B.** Sequences of cDNA from hiPSC clones: clone #24 (mut) expresses c.2133delG allele; clone #5 (WT) expresses WT allele; cDNA from the bulk of mixed 1:1 WT and mut clones ("mosaic") shows the expression of both alleles and a frameshift created by two independent sequences from two clones.

HiPSC were fully characterized by immunostaining and tested for self-renewal and pluripotency properties by trilineage differentiation. All clones had a typical hESC-like morphology (**Figure 12A**) and were able to form embryoid bodies (**Figure 12B**). HiPSC expressed self-renewal markers NANOG and SOX2 (**Figure 12C**). *In vitro* trilineage differentiation confirmed the ability of the clones to spontaneously

differentiate into three germ layers (**Figure 12D**). The staining with anti-PCDH19 antibody showed the localization of the protein in the centrosomes of dividing cells (**Figure 12E**).

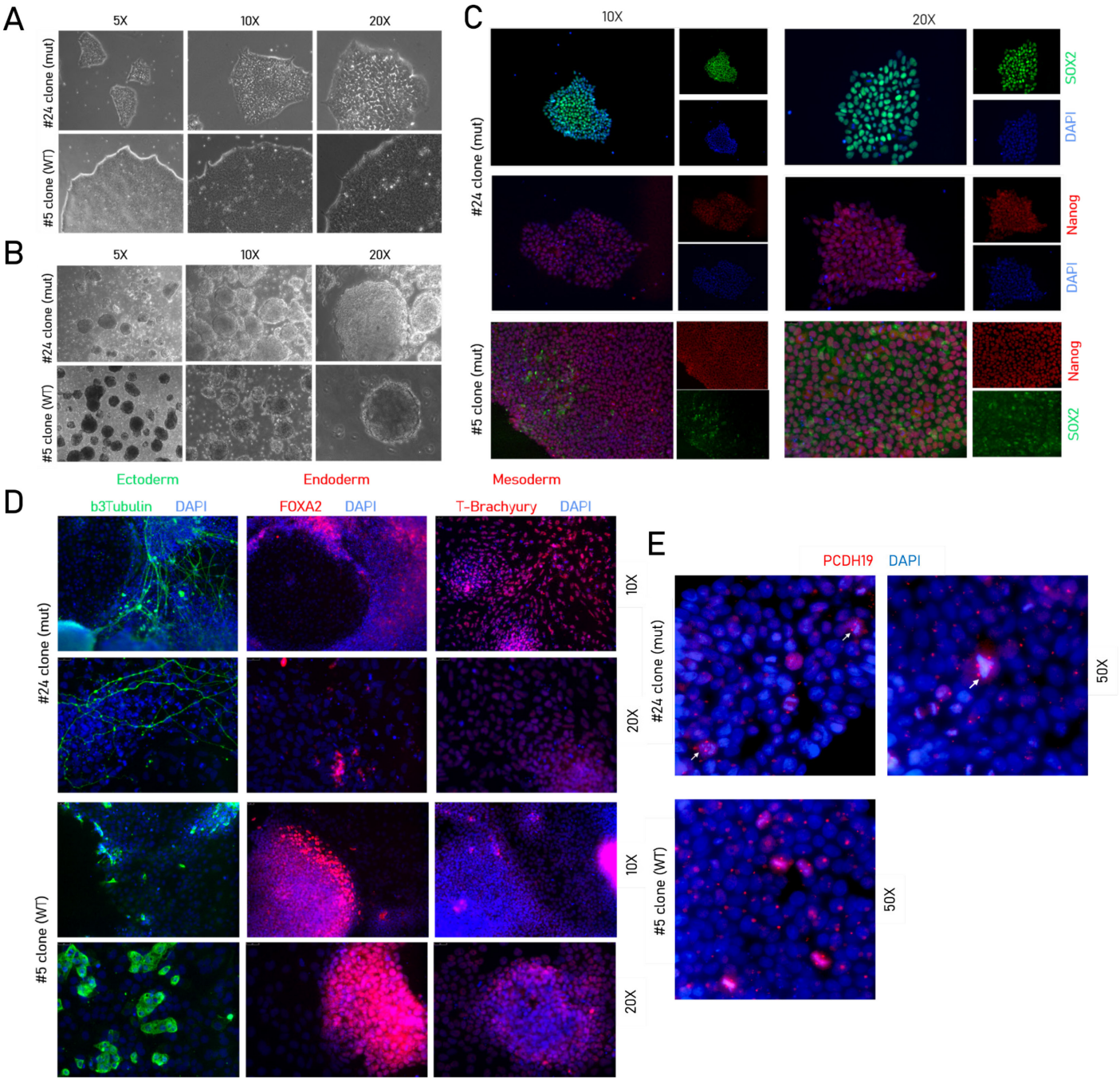

Figure 12. Generation and characterization of hiPSC clones. **Panel A.** Phase contrast images of two hiPSC clones derived from patient (clone #5 (WT) and clone #24 (mut); **Panel B.** Phase contrast images of embryoid bodies (EB) at differentiation day 7; **Panel C.** Immunostaining for self-renewal markers Nanog and SOX; **Panel D.** Immunostaining of hiPSC clones differentiated in three germ layers (β3-tubulin for ectoderm, FOXA2 for endoderm

and T-brachyury for mesoderm) at differentiation day 14. **Panel E.** Immunostaining for PCDH19. Anomalous metaphases in dividing cells of the clone #24 are shown with white arrows.

Neurogenin 2-induced neuronal differentiation of hiPSC

In order to investigate the role of PCDH19 during neurogenesis, mature neurons were obtained from hiPSC through the forced expression of Ngn2. Neuronal differentiation of the generated hiPSC lines: mutated, WT and "mosaic" was assessed by immunostaining (in two independent experiments). Doxycycline-induced GFP expression of differentiated neurons was present from the first day of induction (**Figure 13A**) and all along the experiment. As expected, we observed neuron-like cells starting from DPI 5 (**Figure 13B**). All clones were already β3-tubulin positive starting from DPI 8 (**Figure 13C**) and until the last staining on the DPI 35 (**Figure 13E**). We stained mature neurons for β3-tubulin to assess the differences in neurite length and ramification between clones, the mut clone #24 had more dendrites than the other two clones (**Figure 13E**). To access the maturation rate, we immunostained all three hiPSC lines with mature neuronal marker NeuN starting from DPI 14. Clone #24 were NeuN-positive at DPI 18 while WT clone #5 and mosaic – later, at DPI 24. (**Figure 13D**). HiPSC-derived neurons immunostained with neuronal markers were also GFP positive and easily distinguishable from the DAPI positive rat astrocytes (**Figure 13D, 13E)**.

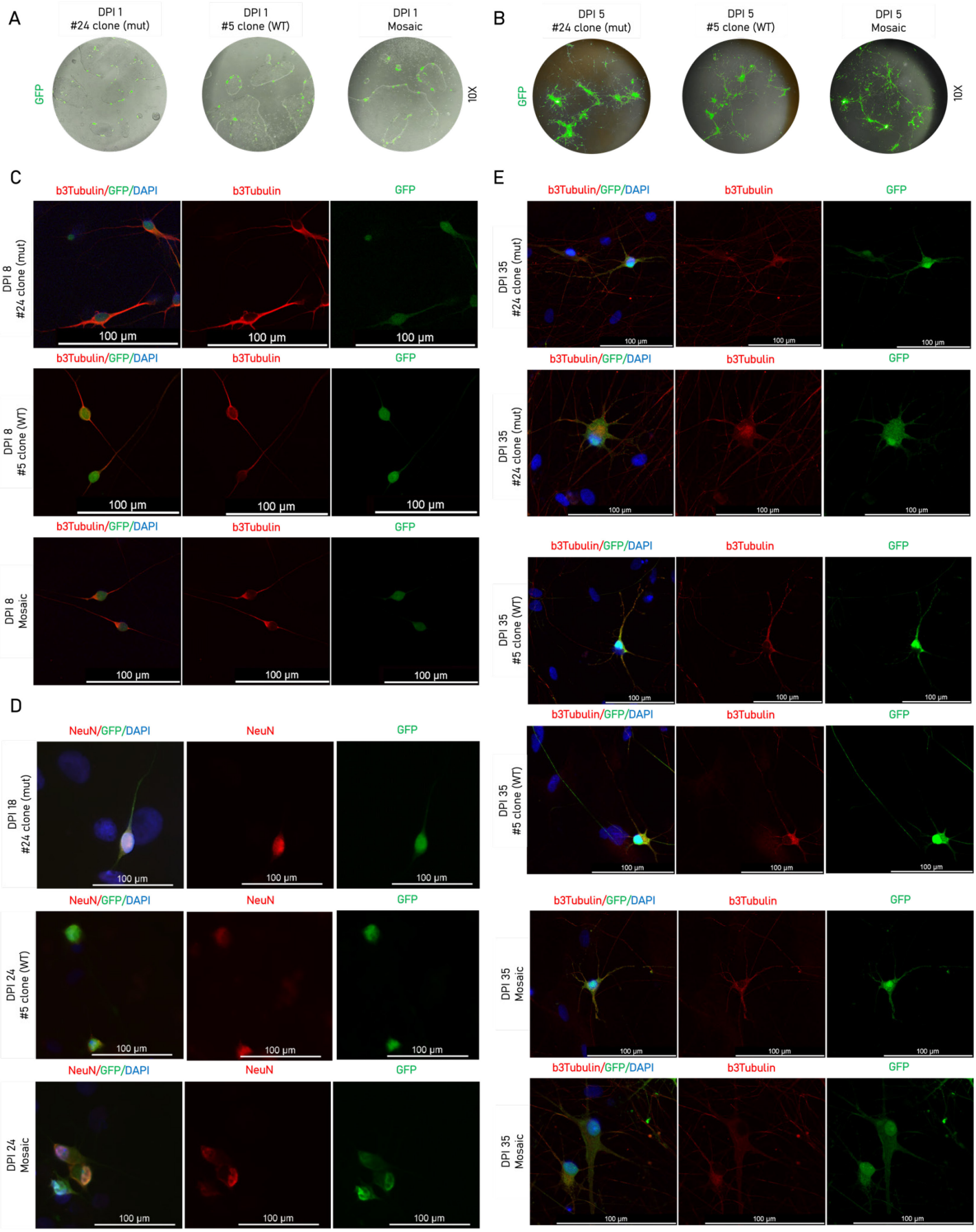
A
DPI 1
#24 clone (mut)
DPI 1
#5 clone (WT)
DPI 1
Mosaic
GFP
10X
B
DPI 5
#24 clone (mut)
DPI 5
#5 clone (WT)
DPI 5
Mosaic
GFP
10X
C
b3Tubulin/GFP/DAPI
b3Tubulin
GFP
DPI 8
#24 clone (mut)
DPI 8
#5 clone (WT)
DPI 8
Mosaic
100 µm
D
NeuN/GFP/DAPI
NeuN
GFP
DPI 18
#24 clone (mut)
DPI 24
#5 clone (WT)
DPI 24
Mosaic
100 µm
E
b3Tubulin/GFP/DAPI
b3Tubulin
GFP
DPI 35
#24 clone (mut)
DPI 35
#24 clone (mut)
DPI 35
#5 clone (WT)
DPI 35
#5 clone (WT)
DPI 35
Mosaic
DPI 35
Mosaic
100 µm

Figure 13. Characterization of Ngn2-induced neurons (n=2). **Panel A.** Phase contrast images of #24 (mut), #5 (WT) and mosaic hiPSC with blue (488 nm) filter after 24h of doxycycline induction at DPI 1. The GFP expression represents successful start of doxycycline induction. **Panel B.** Representative images of neuron-like cells with blue (488 nm) filter at DPI 5. Cells are showing neuron-like morphology. **Panel C.** Immunostaining for β3-tubulin in #24 (mut), #5 (WT) and mosaic hiPSC at DPI 8. GFP expression indicates the doxycycline-induced neurons and distinguishes them from mouse astrocytes. Only induced neurons express a neuronal marker β3-tubulin. **Panel D.** Immunostaining for mature neuronal marker NeuN in clone #24 (mut) at DPI 18, clone #5 (WT) and mosaic hiPSC at DPI 24. Clone #24 (mut) maturated earlier than the other two clones . Rat astrocytes are DAPI positive and GFP negative. **Panel E.** Immunostaining for β3-tubulin in #24 (mut), #5 (WT) and mosaic hiPSC at DPI 35. Rat astrocytes are DAPI positive and GFP negative.

Neuronal excitability of hiPSC-derived neurons

To recreate the mosaic conditions, PCDH19 mut and PCDH19 WT hiPSCs were expanded and mixed in a 1:1 ratio (mosaic neurons). We performed a preliminary current-clamp (**Figure 14**) and voltage-clamp (**Figure 15**) experiments, recording 5-6 neurons for every condition. We revealed some interesting trends, which should be confirmed on a higher number of neurons. However, due to the small number of registrations, the differences may be caused by the state of the neurons from different lines during one single experiment, as we can see on the overall AP traces of the clone #24 (mut) (**Figure 14A**). Therefore, the graph (**Figure 14B)** showed a lowest among three lines AP firing frequency upon depolarizing current injection in the clone #24 (mut) and the highest – in the mosaic neurons. We analyzed the features of the AP evoked by the injection of depolarizing current (**Figure 14C**) and observed increased threshold and lowest AP amplitude in mut neurons (**Figure 14D**). We also observed an increased AP width in mosaic and #24 (mut) clones that, if confirmed, may suggest alterations in AP kinetic (**Figure 14D**).

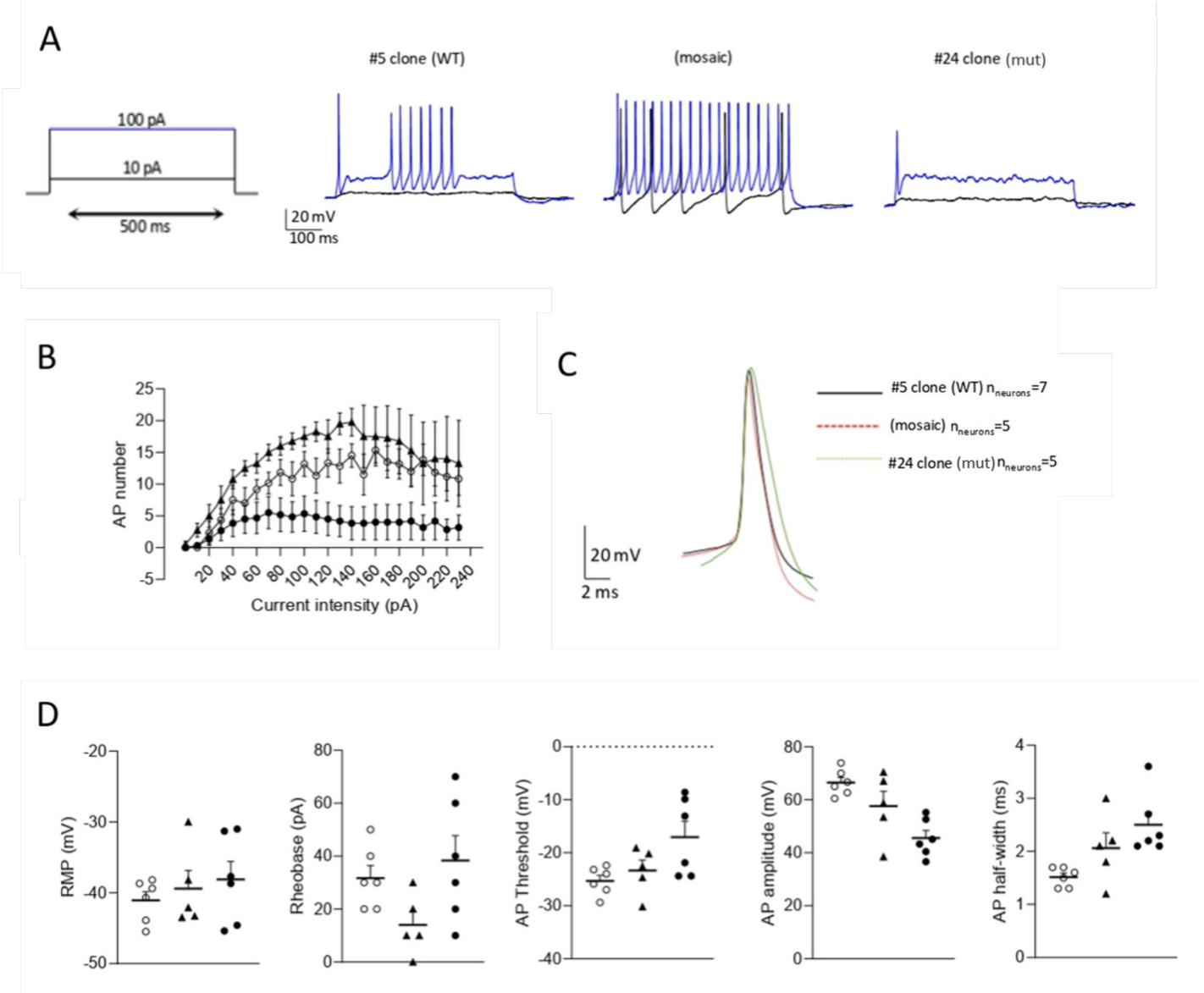

Figure 14. Neuronal excitability in clone #5 (WT), clone #24 (mut) and mosaic (WT+mut) hiPSC. **Panel A.** Representative traces of current-clamp whole-cell experiment; **Panel B.** Graph showing the action potential (AP) frequency in relation to the injected current intensity; **Panel C.** Representative traces of the first AP evoked by injected current; **Panel D.** Histograms showing the resting membrane potential (RMP), the rheobase, the AP threshold, the AP amplitude and the AP half-width (AP duration at the membrane voltage halfway between AP threshold and AP peak) for each clone analyzed.

Voltage-clamp analysis maintains the voltage constant and allows to measure ion movements as electric currents (**Figure 15**). The clamp records reveal an inward current followed by an outward current during step depolarizations [42]. The currents were recorded with depolarization steps ranging from -75mV

a + 85mV in 5 mV (10ms) steps and cells maintained at -65mV. Current densities (**Figure 15B**) are expressed in current divided by capacitance and allow to calculate current densities and compare ionic currents in neurons. In this experiment, we observed the trend of increase in inward and outward currents in mosaic neurons, compared to WT and mut neurons (**Figure 15B, 15C**).

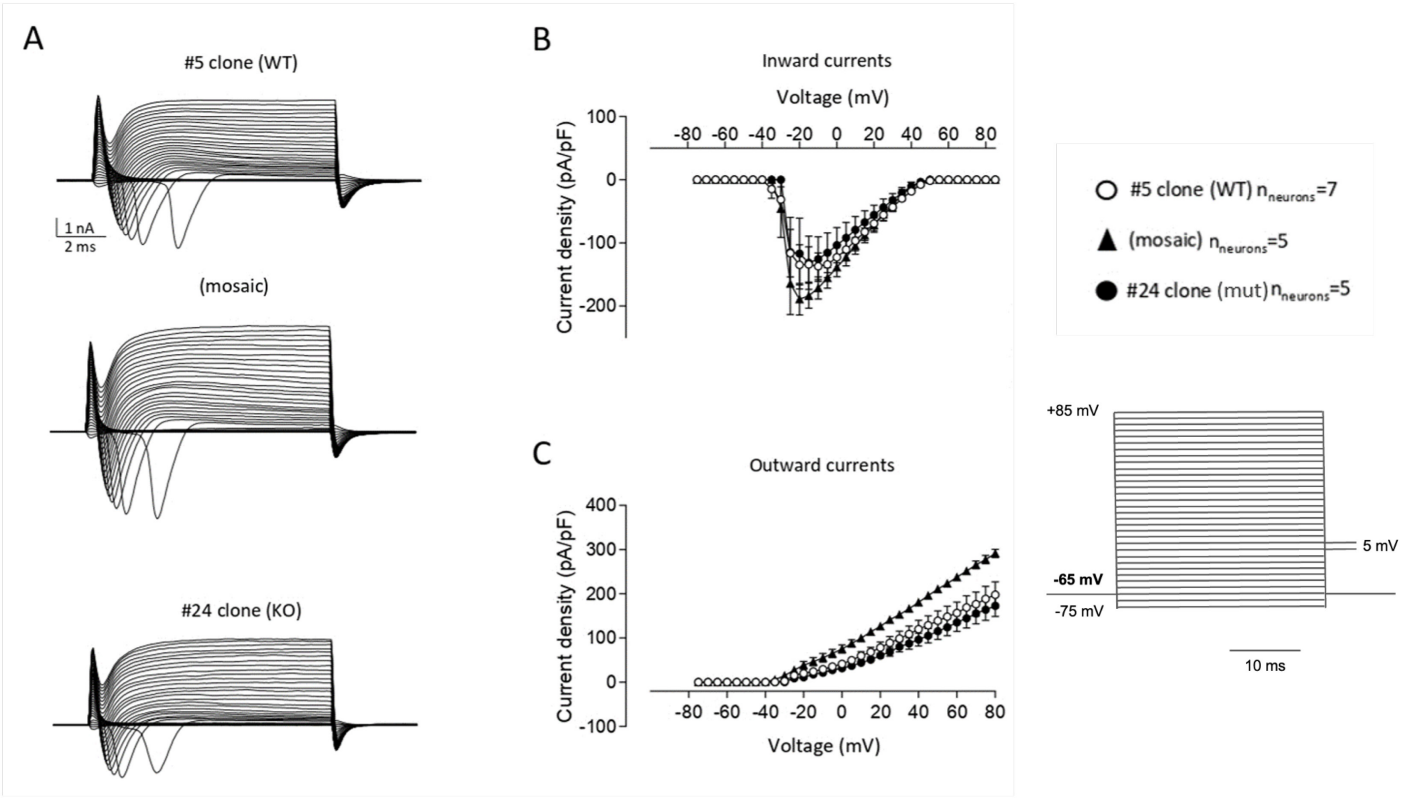

Figure 15. Functional properties of voltage-gated ion channels in clone #5 (WT), clone #24 (mut) and mosaic (WT+mut) hiPSC. **Panel A.** Representative traces of voltage-clamp whole-cell experiment showing inward and outward currents; **Panel B.** Graph showing the inward current voltage relationship of neurons; **Panel C.** Graph showing the outward current voltage relationship of neurons.

Discussion

In this study, we aimed to create a human cellular model of PCDH19-CE obtaining cells from a patient and, in parallel, create an efficient CRISPR/Cas9 strategy for a *PCDH19* knock-out in patients' cells, with a final goal of creating a therapeutic tool for the treatment of PCDH19-CE.

CRISPR/Cas9 gene editing in PCDH19-CE

The editing method that was chosen to achieve the aim is CRISPR/Cas9-mediated deletion of the *PCDH19* gene using a pair of CRISPR sgRNAs targeting the gene. Simultaneous use of dual sgRNAs to target an individual gene was shown to significantly improve the Cas9-mediated genome targeting with a bi-allelic modification efficiency of up to 78% [43]. The *PCDH19* gene contains six, or five exons, where the second one can be alternatively spliced. The major part of mutations predicted to be LOF which can be the whole gene deletions, stop codon mutations, indels, missense and splicing mutations, were reported to be located within the first exon [3], [44]. Also, while protein-truncating mutations are spread throughout the length of the gene, missense and non-synonymous mutations are always located on the extracellular domain of the PCDH19 protein, and there are yet no missense mutations reported in the intracellular part of the protein [45], [46]. We tested different sgRNAs pairs targeting the first exon or the whole gene. Using the sgRNAs flanking the ends of the first exon, we obtained 72,9% transfection efficiency with AAV vectors, and with sgRNAs flanking the first and the last exons (cutting the whole gene) – 48,5% using a lentiviral vector. The efficiency of central nervous system (CNS) gene editing is mainly based on the chosen delivery system. A recombinant viral vector system was considered the best for long-term and stable expression as well as absence of toxicity [47], [48]. For this reason, the usage of AAV and lentiviral vectors for CNS is the most appropriate option even though they have a comparatively low packaging capacity. AAV has higher safety level because of its non-pathogenic nature in wild-type form, ability to induce high transgene expression compared to lentivirus and large vector spread. Lentiviral vectors have been

successfully used to transduce most cell types within the central nervous system (CNS) *in vivo*, including neurons, astrocytes, adult neural stem cells, oligodendrocytes, and glial cells [49–51]. Although, when used *in vitro*, the size of plasmids more than 12 kb can decrease the efficiency of transfection [52]. When large plasmids are used in combination with the electric pulses cell viability is reduced by 30-40% [53]. The size However, the plasmid DNA is evenly distributed in cell suspension while transfected in vitro but may be an obstacle for the in vivo application in tissues where vector particles are administered in small volumes [54]. Taking into account the features present in our plasmids that are only necessary for selection *in vitro*, the size of plasmid for *in vivo* experiments using viral vectors can be significantly reduced, thus increasing the efficiency [55]. The next step will be to test the plasmid in human neurons, analyzing the efficiency and specificity of editing and off-target events, to eventually pass to a murine model of PCDH19-CE.

Generation of PCDH19-CE model from female patient cells

To model *in vitro* PCDH19-CE for which affected neurons are difficult to access, we obtained hiPSCs from female patients' primary fibroblasts and differentiated them into mature neurons using an overexpression of the transcription factor Neurogenin 2. An important point in modeling a neuronal disease is the use of appropriate controls. One option would be those differing from the patient by only studying genetic defect. For instance, it can be achieved by introducing mutations in control cell lines or by restoring the wild-type sequence in a patient cell line [57], [58]. Instead, we generated isogenic cell lines taking advantage of changes in X-inactivation pattern during reprogramming of patients' primary cells into hiPSC. This strategy allowed us to generate hiPSC clones carrying the mutant or the wild-type allele of *PCDH19* gene. It is known that inactive X undergoes chromatin changes during reprogramming, and expansion of hiPSCs can lead to partial loss of XIST RNA [59]. HiPSC clones from patient-derived mosaic fibroblasts can reactivate somatically silenced X-chromosome and undergo random X-inactivation [59]. Due to the changing X-inactivation occurring during reprogramming into hiPSC coming from female cell lines, it is possible to generate hiPSC clones carrying the mutant or the wild-type allele of an X-linked affected gene.

That strategy has proven its advantages in studies modeling Rett syndrome, using female patients with mutations in the X-linked *MeCP2* gene [59], [60] and to model PCDH19-CE, using two female patients with mutations and hemizygous transmitting male [33]. Therefore, we obtained both WT and mutated hiPSC clones from fibroblasts by reprogramming. In PCDH19-CE, high or low percentages of mosaicism due to skewed X-inactivation in female patients, have been suggested to lead to a milder phenotype [2], [61], or asymptomatic [62]. In later studies, no correlation was found [63], [64]. It has also been shown that the prediction of the phenotype, based on the percentage of mosaicism in blood, is not possible, most likely because it does not necessarily represent the percentage of mosaicism in the brain [6]. Considering these data, in our study, after mixing WT and mut hiPSC in a ratio 1:1, we further did not control if the percentage had changed during the experiment.

PCDH19 **c.2133delG mutation alters metaphases in hiPSC**

It is known that PCDH19 protein localizes at the poles of the mitotic spindle in dividing cells [32], altering its orientation during neurogenesis. It interacts with the proteins of centrosome complexes such as y-tubulin and centriolin and its mutations alter the mitotic spindle structures, with a consequent centrosome hyper amplification [34]. We observed multiple dividing cells with 4 and more centrosomes in hiPSC clone with a frameshift mutation while in isogenic WT clone derived from the same patient were present only normal metaphases. It confirms that reprogramming of patient dermal fibroblasts into hiPSC can be used for *in vitro* studies of PCDH19-CE as soon as they represent the involvement of the mutated gene in cellular processes and development.

Neuronal maturation rate in c.2133delG mutated hiPSC-neurons

We studied the neurogenesis in PCDH19-CE hiPSC using a rapid and efficient method of direct differentiation by the overexpression of transcription factor Neurogenin 2. This method provides mature neurons in three weeks and is characterized by low variability and high reproducibility compared to

classical differentiation protocols [31], [65]. In previous studies, it was shown that mutated and mosaic hiPSC-neurons mature earlier than WT and are being born earlier in these cultures – mut and mosaic cultures had a 4-fold increase in the number of neurons relative to WT at the stage of neural rosettes (β3-tubulin positive) and also the neural rosettes appear earlier in mut hiPSCs (day 5 in comparison with day 15 in control and mosaic hPSC) [33], [34]. With the application of Neurogenin-2 forced differentiation of hiPSC, all hiPSC (mut, WT and mosaic) demonstrated neuron-like morphology at the day 5 post infection. They were also β3-tubulin positive at the DPI 8, which is much faster than using the classical differentiation protocols. In our study, we demonstrated that with application of Neurogenin 2 protocol mut neurons maturate earlier than WT. Mutated neurons started to express mature neuronal marker NeuN at DPI 18, while WT neurons – at DPI 24. The average primary neurite length in mut and mosaic hiPSC-neurons have been shown to be significantly longer than in WT [33]. Although we did not perform statistical analysis, by visual examination, we presumed that mutated cells demonstrate more ramified dendrites than WT neurons. Interestingly, in contrast to the literature data, in our experiments mosaic neurons had the same maturation rate as WT neurons. However, these results may depend on mutation present in the neurons or on the changing ratio of mut and WT cells during cell expansion.

Neuronal excitability in PCDH19-CE

It was shown that PCDH19 downregulation reduces the rheobase and increases the frequency of action potential firing, thus indicating neuronal hyperexcitability [24]. Homozygous null mice also do not show increased electrical brain activity, as do heterozygous mice compared to WT controls [46]. We were able to conduct a test experiment, and observed some interesting trends. In particular, we observed the highest frequency of action potential firing in mosaic neurons, compared to mut and WT neurons. In addition, mosaic neurons had the lowest rheobase – they required less current injection to trigger action potentials, which also confirms their hyperexcitability. A trend in increasing inward currents in mosaic neurons means an increase of depolarizing currents. There was also an increase in outward currents in

mosaic neurons which suggests that mosaic neurons are going back to a resting state more quickly because outward currents are necessary to depolarize neurons after AP. In this way they can be excited again in a short time. These preliminary results are in line with neuronal hyperexcitability present in PCDH19-CE and situation in murine disease model but need confirmation on a bigger number of neurons. In the future, we are planning to repeat the differentiation and electrophysiology experiments to obtain statistically significant data, thus providing hiPSC-neurons for testing of developed CRISPR/Cas9 system.

Conclusions

In our study, we designed and tested in patients' cells two different CRISPR/Cas9 delivery systems. Targeting different parts of the *PCDH19* gene, we obtained the best results using the sgRNAs flanking the ends of the first exon, which encodes extracellular domain of the protein. In this case, using AAV-based vector, transfection efficiency was 72,9%, and with sgRNAs flanking the ends of the gene – 48,5% , employing a lentivirus-based vector. As soon as the usage of AAV and lentiviral vectors for CNS is considered the best for long-term and stable expression and for absence of toxicity, the future studies should be focused on the testing of the developed vectors in neurons, and on the application in the *in vivo* murine model of PCDH19-CE.

We set up the conditions for neuronal differentiation of hiPSC using an overexpression with transcriptional factor Neurogenin 2. We demonstrated that *PCDH19* mosaic neurons showed a significantly elevated excitability, representing the situation in PCDH19-CE brain. The mutation c.2133delG in *PCDH19* gene has not yet been described in literature. We confirmed and completed existing data showing that *PCDH19* mutation c.2133delG affects proper metaphases and leads to an increased number of centrosomes in stem cells. This mutation also leads to accelerated rate of neuronal maturation in premature cells. According to these results, we suggest Ngn-2 hiPSC-derived PCDH19 neurons as an informative, efficient, and reproducible experimental tool for understanding the pathogenesis of PCDH19-CE and a suitable approach for use in targeted drug screening strategies.

References

1. Stosser MB, Lindy AS, Butler E, Retterer K, Piccirillo-Stosser CM, Richard G, McKnight DA. High frequency of mosaic pathogenic variants in genes causing epilepsy-related neurodevelopmental disorders. Genet Med. 2018 Apr;20(4):403-410. doi: 10.1038/gim.2017.114.

2. Depienne C, LeGuern E. PCDH19-related infantile epileptic encephalopathy: an unusual X-linked inheritance disorder. Hum Mutat. 2012 Apr;33(4):627-34. doi: 10.1002/humu.22029.

3. Kolc KL, Sadleir LG, Scheffer IE, Ivancevic A, Roberts R, Pham DH, Gecz J. A systematic review and meta-analysis of 271 PCDH19-variant individuals identifies psychiatric comorbidities, and association of seizure onset and disease severity. Mol Psychiatry. 2019 Feb;24(2):241-251. doi: 10.1038/s41380-018-0066-9.

4. Dibbens LM, Tarpey PS, Hynes K, Bayly MA, et al. X-linked protocadherin 19 mutations cause female-limited epilepsy and cognitive impairment. Nat Genet. 2008 Jun;40(6):776-81. doi: 10.1038/ng.149.

5. Depienne C, Bouteiller D, Keren B, Cheuret E, et al. Sporadic infantile epileptic encephalopathy caused by mutations in PCDH19 resembles Dravet syndrome but mainly affects females. PLoS Genet. 2009 Feb;5(2):e1000381. doi: 10.1371/journal.pgen.1000381.

6. de Lange IM, Rump P, Neuteboom RF, Augustijn PB, et al. Male patients affected by mosaic PCDH19 mutations: five new cases. Neurogenetics. 2017 Jul;18(3):147-153. doi: 10.1007/s10048-017-0517-5.

7. Kolc KL, Møller RS, Sadleir LG, Scheffer IE, Kumar R, Gecz J. PCDH19 Pathogenic Variants in Males: Expanding the Phenotypic Spectrum. Adv Exp Med Biol. 2020;1298:177-187. doi: 10.1007/5584_2020_574.

8. Kolc KL, Sadleir LG, Depienne C, Marini C, Scheffer IE, Møller RS, Trivisano M, Specchio N, Pham D, Kumar R, Roberts R, Gecz J. A standardized patient-centered characterization of the phenotypic spectrum of PCDH19 girls clustering epilepsy. Transl Psychiatry. 2020 May 4;10(1):127. doi: 10.1038/s41398-020-0803-0.

9. Samanta D. PCDH19-Related Epilepsy Syndrome: A Comprehensive Clinical Review. Pediatr Neurol. 2020 Apr;105:3-9. doi: 10.1016/j.pediatrneurol.2019.10.009.

10. Lotte J, Bast T, Borusiak P, Coppola A, Cross JH, et al. Effectiveness of antiepileptic therapy in patients with PCDH19 mutations. Seizure. 2016 Feb;35:106-10. doi: 10.1016/j.seizure.2016.01.006.

11. Sadleir LG, Kolc KL, King C, Mefford HC, Dale RC, Gecz J, Scheffer IE. Levetiracetam efficacy in PCDH19 Girls Clustering Epilepsy. Eur J Paediatr Neurol. 2020 Jan;24:142-147. doi: 10.1016/j.ejpn.2019.12.020.

12. Hynes K, Tarpey P, Dibbens LM, Bayly MA, Berkovic SF, et al. Epilepsy and mental retardation limited to females with PCDH19 mutations can present de novo or in single generation families. J Med Genet. 2010 Mar;47(3):211-6. doi: 10.1136/jmg.2009.068817.

13. Carroll D. Genome engineering with targetable nucleases. Annu Rev Biochem. 2014;83:409-39. doi: 10.1146/annurev-biochem-060713-035418.

14. Abrahimi P, Chang WG, Kluger MS, Qyang Y, Tellides G, Saltzman WM, Pober JS. Efficient gene disruption in cultured primary human endothelial cells by CRISPR/Cas9. Circ Res. 2015 Jul 3;117(2):121-8. doi: 10.1161/CIRCRESAHA.117.306290.

15. Yin H, Song CQ, Dorkin JR, Zhu LJ, Li Y, Wu Q, et al. Therapeutic genome editing by combined viral and non-viral delivery of CRISPR system components in vivo. Nat Biotechnol. 2016 Mar;34(3):328-33. doi: 10.1038/nbt.3471.

16. Lu Y, Xue J, Deng T, Zhou X, Yu K, et al. Safety and feasibility of CRISPR-edited T cells in patients with refractory non-small-cell lung cancer. Nat Med. 2020 May;26(5):732-740. doi: 10.1038/s41591-020-0840-5.

17. Russell S, Bennett J, Wellman JA, Chung DC, Yu ZF, et al. Efficacy and safety of voretigene neparvovec (AAV2-hRPE65v2) in patients with RPE65-mediated inherited retinal dystrophy: a randomised, controlled, open-label, phase 3 trial. Lancet. 2017 Aug 26;390(10097):849-860. doi: 10.1016/S0140-6736(17)31868-8.

18. Mendell JR, Al-Zaidy S, Shell R, Arnold WD, Rodino-Klapac LR, et al. Single-Dose Gene-Replacement Therapy for Spinal Muscular Atrophy. N Engl J Med. 2017 Nov 2;377(18):1713-1722. doi: 10.1056/NEJMoa1706198.

19. Schuessler-Lenz M, Enzmann H, Vamvakas S. Regulators' Advice Can Make a Difference: European Medicines Agency Approval of Zynteglo for Beta Thalassemia. Clin Pharmacol Ther. 2020 Mar;107(3):492-494. doi: 10.1002/cpt.1639.

20. Colasante G, Lignani G, Brusco S, Di Berardino C, Carpenter J, et al. dCas9-Based Scn1a Gene Activation Restores Inhibitory Interneuron Excitability and Attenuates Seizures in Dravet Syndrome Mice. Mol Ther. 2020 Jan 8;28(1):235-253. doi: 10.1016/j.ymthe.2019.08.018.

21. Wright AV, Nuñez JK, Doudna JA. Biology and Applications of CRISPR Systems: Harnessing Nature's Toolbox for Genome Engineering. Cell. 2016 Jan 14;164(1-2):29-44. doi: 10.1016/j.cell.2015.12.035.

22. Hsu PD, Lander ES, Zhang F. Development and applications of CRISPR-Cas9 for genome engineering. Cell. 2014 Jun 5;157(6):1262-1278. doi: 10.1016/j.cell.2014.05.010.

23. Mali P, Aach J, Stranges PB, Esvelt KM, Moosburner M, Kosuri S, Yang L, Church GM. CAS9 transcriptional activators for target specificity screening and paired nickases for cooperative genome engineering. Nat Biotechnol. 2013 Sep;31(9):833-8. doi: 10.1038/nbt.2675.

24. Serratto GM, Pizzi E, Murru L, Mazzoleni S, et al. The Epilepsy-Related Protein PCDH19 Regulates Tonic Inhibition, GABAAR Kinetics, and the Intrinsic Excitability of Hippocampal Neurons. Mol Neurobiol. 2020 Dec;57(12):5336-5351. doi: 10.1007/s12035-020-02099-7.

25. Mincheva-Tasheva S, Nieto Guil AF, Homan CC, Gecz J, Thomas PQ. Disrupted Excitatory Synaptic Contacts and Altered Neuronal Network Activity Underpins the Neurological Phenotype in PCDH19-Clustering Epilepsy (PCDH19-CE). Mol Neurobiol. 2021 May;58(5):2005-2018. doi: 10.1007/s12035-020-02242-4.

26. Bassani S, Cwetsch AW, Gerosa L, Serratto GM, Folci A, et al. The female epilepsy protein PCDH19 is a new GABAAR-binding partner that regulates GABAergic transmission as well as migration and morphological maturation of hippocampal neurons. Hum Mol Genet. 2018 Mar 15;27(6):1027-1038. doi: 10.1093/hmg/ddy019.

27. Gerosa L. The activity dependent cleavage and nuclear function of female limited epilepsy protein PCDH19. 2016.

28. Mertens J, Reid D, Lau S, Kim Y, Gage FH. Aging in a Dish: iPSC-Derived and Directly Induced Neurons for Studying Brain Aging and Age-Related Neurodegenerative Diseases. Annu Rev Genet. 2018 Nov 23;52:271-293. doi: 10.1146/annurev-genet-120417-031534.

29. Soliman MA, Aboharb F, Zeltner N, Studer L. Pluripotent stem cells in neuropsychiatric disorders. Mol Psychiatry. 2017 Sep;22(9):1241-1249. doi: 10.1038/mp.2017.40.

30. Niu W, Parent JM. Modeling genetic epilepsies in a dish. Dev Dyn. 2020 Jan;249(1):56-75. doi: 10.1002/dvdy.79.

31. Sterlini B, Fruscione F, Baldassari S, Benfenati F, Zara F, Corradi A. Progress of Induced Pluripotent Stem Cell Technologies to Understand Genetic Epilepsy. Int J Mol Sci. 2020 Jan 12;21(2):482. doi: 10.3390/ijms21020482.

32. Compagnucci C, Petrini S, Higuraschi N, Trivisano M, et al. Characterizing PCDH19 in human induced pluripotent stem cells (iPSCs) and iPSC-derived developing neurons: emerging role of a protein involved in controlling polarity during neurogenesis. Oncotarget. 2015 Sep 29;6(29):26804-13. doi: 10.18632/oncotarget.5757.

33. Homan CC, Pederson S, To TH, Tan C, et al. PCDH19 regulation of neural progenitor cell differentiation suggests asynchrony of neurogenesis as a mechanism contributing to PCDH19 Girls Clustering Epilepsy. Neurobiol Dis. 2018 Aug;116:106-119. doi: 10.1016/j.nbd.2018.05.004.

34. Borghi R, Magliocca V, Petrini S, Conti LA, et al. Dissecting the Role of PCDH19 in Clustering Epilepsy by Exploiting Patient-Specific Models of Neurogenesis. J Clin Med. 2021 Jun 23;10(13):2754. doi: 10.3390/jcm10132754.

35. Zhang Y, Pak C, Han Y, Ahlenius H, et al. Rapid single-step induction of functional neurons from human pluripotent stem cells. Neuron. 2013 Jun 5;78(5):785-98. doi: 10.1016/j.neuron.2013.05.029.

36. Rubio A, Luoni M, Giannelli SG, Radice I, et al. Rapid and efficient CRISPR/Cas9 gene inactivation in human neurons during human pluripotent stem cell differentiation and direct reprogramming. Sci Rep. 2016 Nov 18;6:37540. doi: 10.1038/srep37540.

37. Frega M, van Gestel SH, Linda K, van der Raadt J, et al. Rapid Neuronal Differentiation of Induced Pluripotent Stem Cells for Measuring Network Activity on Micro-electrode Arrays. J Vis Exp. 2017 Jan 8;(119):54900. doi: 10.3791/54900.

38. Kõressaar T, Lepamets M, Kaplinski L, Raime K, Andreson R, Remm M. Primer3_masker: integrating masking of template sequence with primer design software. Bioinformatics. 2018 Jun 1;34(11):1937-1938. doi: 10.1093/bioinformatics/bty036.

39. Kopp P, Jaggi R, Tobler A, Borisch B, et al. Clonal X-inactivation analysis of human tumours using the human androgen receptor gene (HUMARA) polymorphism: a non-radioactive and semiquantitative strategy applicable to fresh and archival tissue. Mol Cell Probes. 1997 Jun;11(3):217-28. doi: 10.1006/mcpr.1997.0099.

40. Dull T, Zufferey R, Kelly M, Mandel RJ, Nguyen M, Trono D, Naldini L. A third-generation lentivirus vector with a conditional packaging system. J Virol. 1998 Nov;72(11):8463-71. doi: 10.1128/JVI.72.11.8463-8471.1998.

41. Vancraeyenest P, Arsenault JT, Li X, Zhu Q, Kobayashi K, Isa K, Isa T, Vanduffel W. Selective Mesoaccumbal Pathway Inactivation Affects Motivation but Not Reinforcement-Based Learning in Macaques. Neuron. 2020 Nov 11;108(3):568-581.e6. doi: 10.1016/j.neuron.2020.07.013.

42. Armstrong CM, Hille B. Voltage-gated ion channels and electrical excitability. Neuron. 1998 Mar;20(3):371-80. doi: 10.1016/s0896-6273(00)80981-2.

43. Zhou J, Wang J, Shen B, Chen L, Su Y, Yang J, Zhang W, Tian X, Huang X. Dual sgRNAs facilitate CRISPR/Cas9-mediated mouse genome targeting. FEBS J. 2014 Apr;281(7):1717-25. doi: 10.1111/febs.12735.

44. Niazi R, Fanning EA, Depienne C, Sarmady M, Abou Tayoun AN. A mutation update for the PCDH19 gene causing early-onset epilepsy in females with an unusual expression pattern. Hum Mutat. 2019 Mar;40(3):243-257. doi: 10.1002/humu.23701.

45. Gecz J, Thomas PQ. Disentangling the paradox of the PCDH19 clustering epilepsy, a disorder of cellular mosaics. Curr Opin Genet Dev. 2020 Dec;65:169-175. doi: 10.1016/j.gde.2020.06.012.

46. Pederick DT, Richards KL, Piltz SG, Kumar R, et al. Abnormal Cell Sorting Underlies the Unique X-Linked Inheritance of PCDH19 Epilepsy. Neuron. 2018 Jan 3;97(1):59-66.e5. doi: 10.1016/j.neuron.2017.12.005.

47. Choudhury SR, Hudry E, Maguire CA, Sena-Esteves M, Breakefield XO, Grandi P. Viral vectors for therapy of neurologic diseases. Neuropharmacology. 2017 Jul 1;120:63-80. doi: 10.1016/j.neuropharm.2016.02.013.

48. Nobre RJ, Almeida LP. Gene therapy for Parkinson's and Alzheimer's diseases: from the bench to clinical trials. Curr Pharm Des. 2011;17(31):3434-45. doi: 10.2174/138161211798072472.

49. van Hooijdonk LW, Ichwan M, Dijkmans TF, Schouten TG, de Backer MW, Adan RA, Verbeek FJ, Vreugdenhil E, Fitzsimons CP. Lentivirus-mediated transgene delivery to the hippocampus reveals sub-field specific differences in expression. BMC Neurosci. 2009 Jan 13;10:2. doi: 10.1186/1471-2202-10-2.

50. Logan AC, Lutzko C, Kohn DB. Advances in lentiviral vector design for gene-modification of hematopoietic stem cells. Curr Opin Biotechnol. 2002 Oct;13(5):429-36. doi: 10.1016/s0958-1669(02)00346-4.

51. Varma N, Janic B, Ali M, Iskander A, Arbab A. Lentiviral Based Gene Transduction and Promoter Studies in Human Hematopoietic Stem Cells (hHSCs). J Stem Cells Regen Med. 2011 Apr 1;7(1):41-53. doi: 10.46582/jsrm.0701005.

52. Campeau P, Chapdelaine P, Seigneurin-Venin S, Massie B, Tremblay JP. Transfection of large plasmids in primary human myoblasts. Gene Ther. 2001 Sep;8(18):1387-94. doi: 10.1038/sj.gt.3301532.

53. Lesueur LL, Mir LM, André FM. Overcoming the Specific Toxicity of Large Plasmids Electrotransfer in Primary Cells In Vitro. Mol Ther Nucleic Acids. 2016 Mar 8;5(3):e291. doi: 10.1038/mtna.2016.4.

54. Sachdev S, Potočnik T, Rems L, Miklavčič D. Revisiting the role of pulsed electric fields in overcoming the barriers to in vivo gene electrotransfer. Bioelectrochemistry. 2022 Apr;144:107994. doi: 10.1016/j.bioelechem.2021.107994.

55. Hwang LH, Gilboa E. Expression of genes introduced into cells by retroviral infection is more efficient than that of genes introduced into cells by DNA transfection. J Virol. 1984 May;50(2):417-24. doi: 10.1128/JVI.50.2.417-424.1984.

56. Soldner F, Laganière J, Cheng AW, Hockemeyer D, et al. Generation of isogenic pluripotent stem cells differing exclusively at two early onset Parkinson point mutations. Cell. 2011 Jul 22;146(2):318-31. doi: 10.1016/j.cell.2011.06.019.

57. Liu GH, Suzuki K, Qu J, Sancho-Martinez I, et al. Targeted gene correction of laminopathy-associated LMNA mutations in patient-specific iPSCs. Cell Stem Cell. 2011 Jun 3;8(6):688-94. doi: 10.1016/j.stem.2011.04.019.

58. Tchieu J, Kuoy E, Chin MH, Trinh H, et al. Female human iPSCs retain an inactive X chromosome. Cell Stem Cell. 2010 Sep 3;7(3):329-42. doi: 10.1016/j.stem.2010.06.024.

59. Marchetto MC, Carromeu C, Acab A, Yu D, et al. A model for neural development and treatment of Rett syndrome using human induced pluripotent stem cells. Cell. 2010 Nov 12;143(4):527-39. doi: 10.1016/j.cell.2010.10.016.

60. Cheung AY, Horvath LM, Grafodatskaya D, Pasceri P, et al. Isolation of MECP2-null Rett Syndrome patient hiPS cells and isogenic controls through X-chromosome inactivation. Hum Mol Genet. 2011 Jun 1;20(11):2103-15. doi: 10.1093/hmg/ddr093.

61. Depienne C, Trouillard O, Bouteiller D, Gourfinkel-An I, et al. Mutations and deletions in PCDH19 account for various familial or isolated epilepsies in females. Hum Mutat. 2011 Jan;32(1):E1959-75. doi: 10.1002/humu.21373.

62. Dimova PS, Kirov A, Todorova A, Todorov T, Mitev V. A novel PCDH19 mutation inherited from an unaffected mother. Pediatr Neurol. 2012 Jun;46(6):397-400. doi: 10.1016/j.pediatrneurol.2012.03.004.

63. Leonardi E, Sartori S, Vecchi M, Bettella E, et al. Identification of four novel PCDH19 Mutations and prediction of their functional impact. Ann Hum Genet. 2014 Nov;78(6):389-98. doi: 10.1111/ahg.12082.

64. Marini C, Mei D, Parmeggiani L, Norci V, et al. Protocadherin 19 mutations in girls with infantile-onset epilepsy. Neurology. 2010 Aug 17;75(7):646-53. doi: 10.1212/WNL.0b013e3181ed9e67.

65. Meijer M, Rehbach K, Brunner JW, Classen JA, et al. A Single-Cell Model for Synaptic Transmission and Plasticity in Human iPSC-Derived Neurons. Cell Rep. 2019 May 14;27(7):2199-2211.e6. doi: 10.1016/j.celrep.2019.04.058.